



ARL-TR-7733 • AUG 2016



Warrior Injury Assessment Manikin (WIAMan) Lumbar Spine Model Validation: Development, Testing, and Analysis of Physical and Computational Models of the WIAMan Lumbar Spine Materials Demonstrator

**by Michael W Gibson, Robert S Armiger, Paul J Biermann,
Michael P Boyle, Alexander S Iwaskiw, Andrew M Lennon,
Andrew C Merkle, Connor O Pyles, Drew P Seker, Nicholas A
Vavalle, Zhiyong Xia, Jiangyue Zhang, Dawn M Crawford, and
Mostafiz R Chowdhury**

Approved for public release; distribution is unlimited.

NOTICES

Disclaimers

The findings in this report are not to be construed as an official Department of the Army position unless so designated by other authorized documents.

Citation of manufacturer's or trade names does not constitute an official endorsement or approval of the use thereof.

Destroy this report when it is no longer needed. Do not return it to the originator.



Warrior Injury Assessment Manikin (WIAMan) Lumbar Spine Model Validation: Development, Testing, and Analysis of Physical and Computational Models of the WIAMan Lumbar Spine Materials Demonstrator

**Michael W Gibson, Robert S Armiger, Paul J Biermann,
Michael P Boyle, Alexander S Iwaskiw,
Andrew M Lennon, Andrew C Merkle, Connor O Pyles, Drew P
Seker, Nicholas A Vavalle, Zhiyong Xia, and Jiangyue Zhang**
Johns Hopkins Applied Physics Laboratory, Laurel, MD

Dawn M Crawford and Mostafiz R Chowdhury
Weapons and Materials Research Directorate, ARL

REPORT DOCUMENTATION PAGE

Form Approved
OMB No. 0704-0188

Public reporting burden for this collection of information is estimated to average 1 hour per response, including the time for reviewing instructions, searching existing data sources, gathering and maintaining the data needed, and completing and reviewing the collection information. Send comments regarding this burden estimate or any other aspect of this collection of information, including suggestions for reducing the burden, to Department of Defense, Washington Headquarters Services, Directorate for Information Operations and Reports (0704-0188), 1215 Jefferson Davis Highway, Suite 1204, Arlington, VA 22202-4302. Respondents should be aware that notwithstanding any other provision of law, no person shall be subject to any penalty for failing to comply with a collection of information if it does not display a currently valid OMB control number.

PLEASE DO NOT RETURN YOUR FORM TO THE ABOVE ADDRESS.

1. REPORT DATE (DD-MM-YYYY) August 2016		2. REPORT TYPE Technical Report		3. DATES COVERED (From - To) 1 January 2015–31 December 2015	
4. TITLE AND SUBTITLE Warrior Injury Assessment Manikin (WIAMan) Lumbar Spine Model Validation: Development, Testing, and Analysis of Physical and Computational Models of the WIAMan Lumbar Spine Materials Demonstrator				5a. CONTRACT NUMBER	
				5b. GRANT NUMBER	
				5c. PROGRAM ELEMENT NUMBER	
6. AUTHOR(S) Michael W Gibson, Robert S Armiger, Paul J Biermann, Michael P Boyle, Alexander S Iwaskiw, Andrew M Lennon, Andrew C Merkle, Connor O Pyles, Drew P Seker, Nicholas A Vavalle, Zhiyong Xia, Jianguyue Zhang, Dawn Crawford, and Mostafiz Chowdhury				5d. PROJECT NUMBER N00024-13-D-6400	
				5e. TASK NUMBER	
				5f. WORK UNIT NUMBER	
7. PERFORMING ORGANIZATION NAME(S) AND ADDRESS(ES) US Army Research Laboratory ATTN: RDRL-DPW Aberdeen Proving Ground, MD 21005-5069				8. PERFORMING ORGANIZATION REPORT NUMBER ARL-TR-7733	
9. SPONSORING/MONITORING AGENCY NAME(S) AND ADDRESS(ES) WIAMan Engineering Office US Army Research Laboratory Aberdeen Proving Ground, MD 21005				10. SPONSOR/MONITOR'S ACRONYM(S)	
				11. SPONSOR/MONITOR'S REPORT NUMBER(S)	
12. DISTRIBUTION/AVAILABILITY STATEMENT Approved for public release; distribution is unlimited.					
13. SUPPLEMENTARY NOTES					
14. ABSTRACT This report describes the development, testing, and finite element model (FEM) of the Warrior Injury Assessment Manikin (WIAMan) Anthropomorphic Test Device (ATD) Lumbar Spine Materials Demonstrator. A primary objective of this work was to generate experimental data for FEM validation and to create lumbar spine demonstrators that were used to characterize candidate materials to assess the effect of material type and hardness for the lumbar spine ATD component. Several rubber chemistries and hardnesses were used for the compliant elements of the lumbar spine demonstrators. The material demonstrators were tested under dynamic loading using the Medical College of Wisconsin vertical accelerator test machine. The responses of the different lumbar spine demonstrators were compared with the biofidelic response corridors to assess the levels of biofidelity of the WIAMan ATD lumbar spine design.					
15. SUBJECT TERMS lumbar spine, model validation, testing and analysis, WIAMan spine model, biofidelic response corridors, vertical accelerator, compliant element, rubber					
16. SECURITY CLASSIFICATION OF:			17. LIMITATION OF ABSTRACT UU	18. NUMBER OF PAGES 70	19a. NAME OF RESPONSIBLE PERSON Patricia A Riippa
a. REPORT Unclassified	b. ABSTRACT Unclassified	c. THIS PAGE Unclassified			19b. TELEPHONE NUMBER (Include area code) 410-278-2156

Standard Form 298 (Rev. 8/98)
Prescribed by ANSI Std. Z39.18

Approved for public release; distribution is unlimited.

Contents

List of Figures	v
List of Tables	vi
Executive Summary	vii
1. Introduction	1
1.1 WIAMan Project	1
1.2 Lumbar Spine Materials Demonstrator	1
1.2.1 WIAMan ATD Lumbar Spine Assembly	1
1.2.2 Materials Consideration	2
1.2.3 Test Method	3
2. Preliminary Modeling and Simulation	3
2.1 VertAc Rig Model Validation	3
2.2 Preliminary Material Optimization	6
3. Materials Characterization	8
3.1 Material Selection	8
3.2 Material Characterization Testing	11
3.2.1 Compression Testing	11
3.2.2 Tension Testing	14
3.2.3 Combined Results	17
4. Fabrication Efforts	18
4.1 TDP Design	18
4.2 Lumbar Spine Assembly	18
4.2.1 Assembly Method	20
4.2.2 Adhesive Testing	22
4.3 VertAc Rig Interface and Mass Compensation	26
5. Materials Demonstrator Testing	27

5.1	VertAc Overview	27
5.2	VertAc Test Method	28
5.3	VertAc Test Instrumentation	30
5.4	VertAc Test Results	31
6.	Modeling and Simulation Validation	41
6.1	Model Refinement	41
6.2	Model Correlation to VertAc Test Results	43
6.3	Model Predictive Results	45
6.4	Model Correlation to BRCs	46
7.	Conclusions and Recommendations	48
8.	References	50
	Appendix. Additional Testing Data	51
	List of Symbols, Abbreviations, and Acronyms	57
	Distribution List	59

List of Figures

Fig. 1	WIAMan ATD lumbar spine design.....	2
Fig. 2	Hybrid-III lumbar spine in VertAc rig.....	5
Fig. 3	VertAc rig validation cases.....	6
Fig. 4	Optimized ATD lumbar spine force transmission results.....	7
Fig. 5	Comparison of force transmission predictions.....	7
Fig. 6	DMA master curves.....	9
Fig. 7	Compression sample with lubricated platens.....	13
Fig. 8	Custom fixture for high-rate testing.....	15
Fig. 9	Shortened test sample for high-rate (50 s ⁻¹) tension testing.....	16
Fig. 10	X-intercept method with stress strain curve to achieve strain shift.....	17
Fig. 11	Combined average stress stain curves.....	18
Fig. 12	Lumbar spine per Humanetics drawing 130-4120.....	19
Fig. 13	Lumbar spine assembly in alignment fixture.....	22
Fig. 14	Double-lap shear coupons before and after testing.....	23
Fig. 15	Initial lap-shear testing results.....	24
Fig. 16	Additional lap-shear testing results.....	25
Fig. 17	Lumbar spine with VertAc rig interface blocks.....	26
Fig. 18	Lumbar spine materials demonstrator mounted in VertAc rig.....	28
Fig. 19	VertAc pretest matrix.....	29
Fig. 20	VertAc rig instrumentation.....	30
Fig. 21	Intracomponent repeatability.....	32
Fig. 22	Intercomponent repeatability.....	33
Fig. 23	Response sensitivity to compliant material.....	34
Fig. 24	Response sensitivity to impact speed.....	34
Fig. 25	Mass compensation of lumbar spine VertAc data.....	35
Fig. 26	Moment transformation of lumbar spine VertAc data.....	36
Fig. 27	Moment transformation dimensions in X and Y.....	36
Fig. 28	Moment transformation dimensions in Z.....	37
Fig. 29	Vertical force responses at L1/T12 compared to BRC for 1.2 m/s.....	38
Fig. 30	Moment responses at L1/T12 compared to BRC for 1.2 m/s.....	38
Fig. 31	WIAMan lumbar spine FEM.....	42

Fig. 32	Single element stress-strain results for EPDM 60 Shore A	43
Fig. 33	EPDM 60 simulation results summary	44
Fig. 34	Ogden viscoelastic simulation results summary	44
Fig. 35	ATD peak force compared to BRC peak force	47
Fig. 36	Results of varying material type at each spinal level.....	48

List of Tables

Table 1	VertAc and Hybrid-III material properties	4
Table 2	VertAc rig validation using Hybrid-III FEM; CORA scores.....	5
Table 3	Lumbar spine rubber optimization against L1 force BRCs; CORA scores.....	7
Table 4	Thermal and thermomechanical results	10
Table 5	Formulation details for PBD/NR	10
Table 6	Formulation details for EPDM.....	11
Table 7	Single material test matrix (butyl rubber) for compression	12
Table 8	Average achieved strain rates for compression	13
Table 9	Single material test matrix (butyl rubber) for tension.....	14
Table 10	Average achieved strain rates for tension	16
Table 11	Materials specified for lumbar spine components in TDP.....	19
Table 12	Ballast plate mass comparison	27
Table 13	VertAc test matrix.....	29
Table 14	MCW testing data channels	31
Table 15	MCW testing overall CORA scores for comparison to BRCs.....	40
Table 16	MCW testing size CORA scores for comparison to BRCs.....	41
Table 17	Simulation matrix for material exploration.....	43
Table 18	Blind validation experiments	45
Table 19	L1 force CORA score breakdown for blind validation cases	46
Table 20	L1 Moment CORA score breakdown for blind validation cases	46

Executive Summary

This report provides background and details on the development, testing, and analysis of the physical and finite element model (FEM) of the Warrior Injury Assessment Manikin (WIAMan) Anthropomorphic Test Device (ATD) Lumbar Spine Materials Demonstrator. This effort had 3 main objectives, the first of which was to generate experimental data that could be used for FEM validation. This primary objective was achieved through the use of the outcome of the second objective, which was to create Lumbar Spine Materials Demonstrators that could be used to characterize candidate materials and evaluate the sensitivity of the ATD lumbar spine response to material parameters. Testing these materials demonstrators provided the experimental data required for FEM validation. The third objective was to compare the materials demonstrators' responses against the Biofidelic Response Corridors (BRCs) to determine the level of biofidelity of the ATD lumbar spine design.

The path taken to achieve these objectives required several steps. These steps included using the FEM for preliminary material optimization, selecting compliant materials for testing, fabricating ATD Lumbar Spine Materials Demonstrators, testing materials and materials demonstrators in a dynamic loading environment, and comparing materials demonstrator responses to FEM simulation outputs and the BRCs. Preliminary material optimization with the FEM pointed towards a compliant material Shore A hardness of around 65. Several materials demonstrators were fabricated with varying hardnesses and compliant material families and were subjected to dynamic loading using the Medical College of Wisconsin's vertical accelerator (VertAc). The FEM simulations compared well with the VertAc test data, with the Ogden viscoelastic material model having the best correlation to the test data. The peak force VertAc test data and FEM simulation output were also compared to the BRCs. Both indicated that a material hardness of around 60A would be the closest match to the peak force BRCs. While moment VertAc test data and moment FEM simulation outputs compared well with each other, the moment data and output did not compare well with moment BRCs. The importance of the moment will be better understood after the planned postmortem human subject alternate posture testing is completed. Plots comparing the VertAc test data and FEM simulation output to the BRCs are provided in this report.

It is recommended that the validated FEM model be used to optimize the compliant material and the geometry of the WIAMan ATD lumbar spine to match the BRCs, and that the optimized design be built and subjected to a dynamic loading environment to confirm the response predicted by the FEM simulations.

1. Introduction

1.1 WIAMan Project

The United States Department of Defense (DOD) has acknowledged that current methods used to assess combat vehicle occupant injuries from an under-body blast (UBB) are inadequate. Specifically, existing anthropomorphic test devices (ATDs) and associated injury criteria were neither designed for nor capable of accurately predicting human response and subsequent injuries in a vertical loading environment. The ATDs currently in use were originally developed by the automotive industry and designed for frontal-, rear-, or side-impact crashes. These test devices were designed for these specific applications and were not intended to be biofidelic in UBB conditions.

To address the limitations of existing technology, the DOD commissioned the Warrior Injury Assessment Manikin (WIAMan) Project. The purpose of this project is to create a warrior-representative ATD for the live-fire environment, which will be biofidelic in both its initial response to UBB loading and its ability to provide a sensitive and specific injury assessment capability. The ultimate goal is to improve occupant protection and survivability in a UBB event.

1.2 Lumbar Spine Materials Demonstrator

Finite element models (FEMs) are being used to help evaluate and inform any future redesign of the WIAMan ATD Concept Demonstrator. To ensure that the FEMs are accurately representing the response of the actual ATD components, these models need to be validated against experimental data. To this end, a Lumbar Spine Materials Demonstrator was fabricated to 1) provide experimental data for FEM validation and 2) permit the investigation of lumbar spine response due to materials selection.

1.2.1 WIAMan ATD Lumbar Spine Assembly

The lumbar spine is an assembly of 2 aluminum mounting plates, 2 aluminum discs, and 3 rubber pucks, which are assembled by adhesive bonding. An image of the computer-aided design (CAD) 3-D model of the Lumbar Spine Concept Demonstrator lumbar spine, with callouts of each component, is shown in Fig. 1.

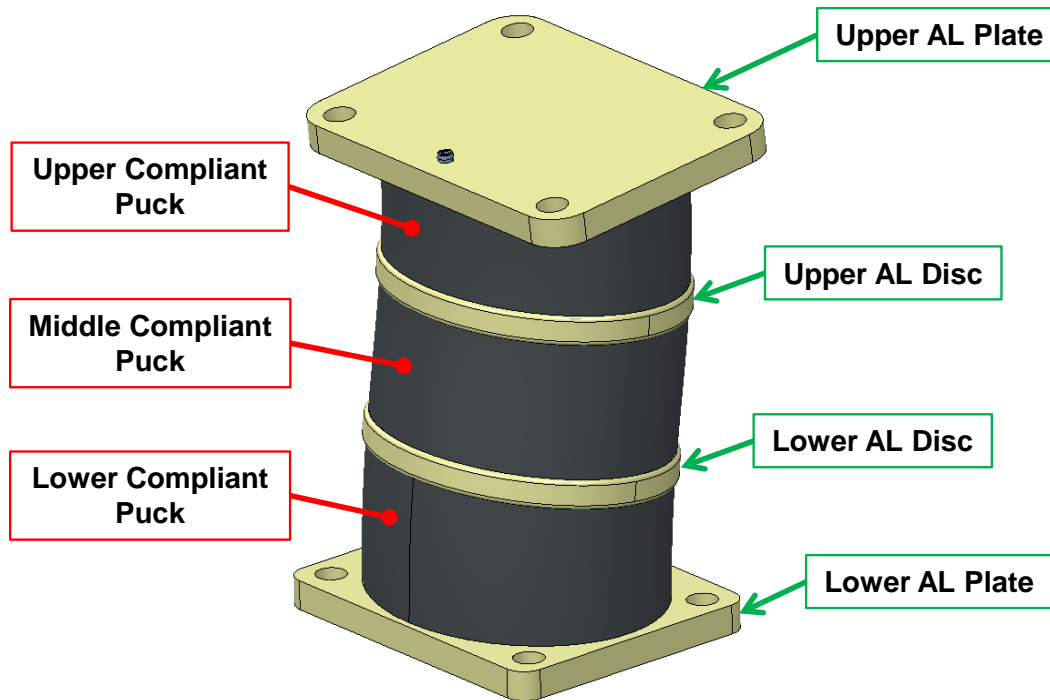


Fig. 1 WIAMan ATD lumbar spine design

1.2.2 Materials Consideration

To aid in validation of the FEM, Lumbar Spine Materials Demonstrators were fabricated to assess candidate material options. The input to the FEM simulations had to be the same as the loading conditions that the lumbar spine assemblies were subjected to. The original Humanetics technical data package (TDP) for the WIAMan ATD Concept Demonstrator specifies 7075-T6 aluminum for the aluminum parts and neoprene with a Shore A hardness of 75 for the rubber pucks.¹ Neoprene is known to degrade over time, so other compliant materials were also selected for evaluation.

Selecting a new compliant material to replace the neoprene involved researching various rubber materials and characterizing their material properties. Part of this research included considering compliant materials used in other parts of the ATD and using the FEM for preliminary material optimization. As a result of this research, 2 different rubber families and 3 different rubber hardnesses were selected to use for testing and validation of the FEM. The processes involved in this preliminary material optimization and selection will be discussed in greater detail later in this report. Once the materials were selected for testing, 6 Lumbar Spine Materials Demonstrators were fabricated.

1.2.3 Test Method

The materials demonstrators were subjected to the same loads used to generate the biofidelic response corridors (BRCs) for the WIAMan ATD lumbar spine. The BRCs define various response characteristics of specific human cadaveric components during specified events. In the case of the lumbar spine, the event was the lumbar spine being oriented in its neutral position and then being hit from below at various impact speeds. The responses for this case included the vertical force at the top and bottom of the lumbar spine and the moment at the top and bottom of the lumbar spine. The BRCs were generated from postmortem human subject (PMHS) testing of lumbar spines in their neutral position on the vertical accelerator (VertAc) at the Medical College of Wisconsin (MCW). Samples of the selected compliant materials were also subjected to material characterization testing at the Johns Hopkins University Applied Physics Laboratory (JHU/APL) to determine their material properties. The data from the material characterization testing were used to improve the material models used in the ATD lumbar spine FEM.

The data obtained from the VertAc testing were then compared to the FEM simulation output to validate the model. This validated model could then be used to further inform the design of the ATD. The VertAc test data were also compared to the BRCs to determine how close the preliminary material optimization came to matching the BRCs. Further details of the validation of the lumbar spine model are provided in the following sections.

2. Preliminary Modeling and Simulation

2.1 VertAc Rig Model Validation

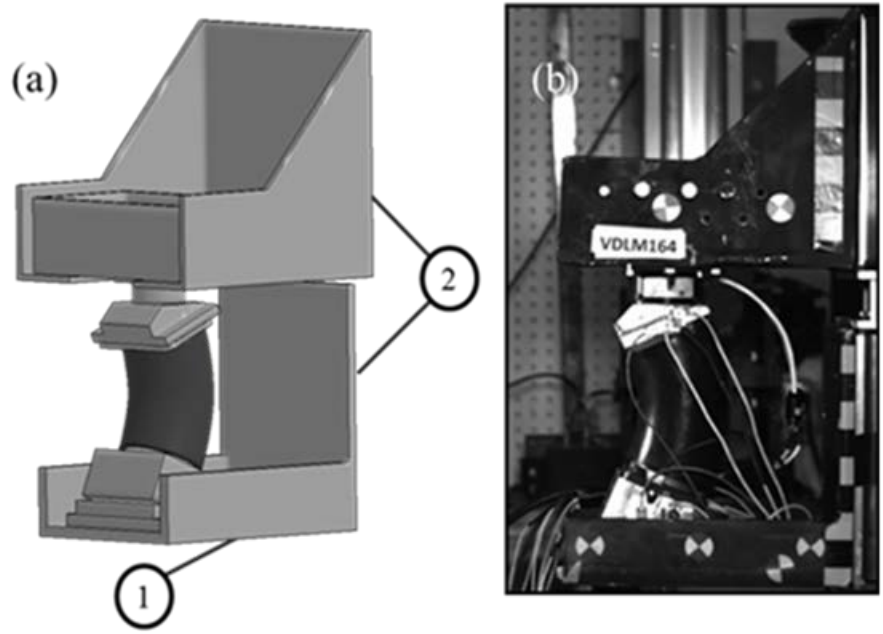
Validation of model boundary conditions must be performed to gain confidence in predicted results. To this end, an explicit FEM of MCW's VertAc test rig was developed and validated in LS-DYNA (Livermore Software Technology Corporation) to ensure proper loading of the WIAMan lumbar spine FEM. Model geometry was defined according to CAD drawings provided by MCW and was meshed in Cubit (Sandia National Laboratories) using solid hexahedral elements. For this rig validation, a Hybrid-III (the current automotive industry standard ATD, designed and built by Humanetics) lumbar spine was used, as data from VertAc tests were available for comparison. Material properties and how these properties were implemented for each component of the simulation are provided in Table 1.

Table 1 VertAc and Hybrid-III material properties

Physical material	Numerical implementation	Parameters
6061 aluminum	Linear elastic	E = 68.9 GPa $\rho = 2,700 \text{ kg/m}^3$
1018 steel	Linear elastic	E = 205.0 GPa $\rho = 7,870 \text{ kg/m}^3$
Hybrid-III lumbar Spine rubber	Blatz-Ko	G = 10.0 MPa $\rho = 2,050 \text{ kg/m}^3$

Linear-elastic material models were selected to characterize all steel and aluminum components, and a Blatz-Ko model was used for the rubber elements of the Hybrid-III lumbar spine. These efficient linear-elastic models were able to be used instead of material models that included plastic-strain and time or temperature dependence because none of the elements reached their yield stress during any of the VertAc simulations described in this report. Following material model assignment, a comparison of FEM simulated mass to physical mass resulted in a difference of less than 0.55%.

The VertAc FEM was validated by simulating vertical loading of a Hybrid-III lumbar spine FEM and comparing transmitted force to analogous experiments conducted with a Hybrid-III lumbar spine at MCW. The Hybrid-III lumbar spine FEM was adapted from LSTC's Hybrid-III 50th Percentile Dummy FEM, with a Blatz-Ko constitutive model introduced to represent the 80 Shore A polyacrylate lumbar spine rubber. Validation cases were simulated under 2 unique loading conditions, with lower carriage velocities reaching peaks of 1.2 and 2.4 m/s, respectively. All VertAc simulations described in this report were test-specific, meaning no average boundary conditions were created, the simulations had their kinematics prescribed at the lower carriage according to experimentally measured carriage accelerations (DTS 6DX Pro), and the simulations were constrained to move in the vertical direction at the posterior linear-bearings. Side-by-side images of the Hybrid-III lumbar spine in the MCW VertAc rig (both the FEM and during testing at MCW) are provided in Fig. 2.



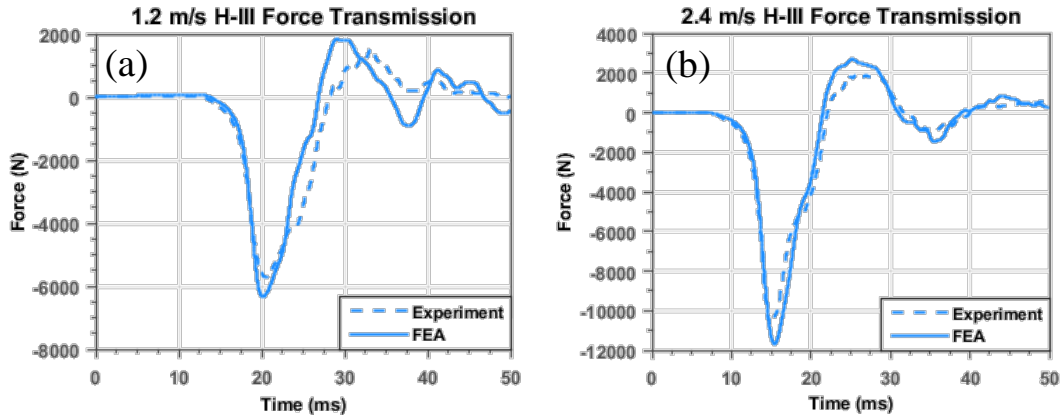
Note: a) Finite element model of the Hybrid-III 50th percentile lumbar spine in the VertAc rig model. Boundary velocities were applied to the lower carriage (a-1), while the rears of both carriages (a-2) were constrained to move in the vertical direction. b) VertAc test setup at MCW.

Fig. 2 Hybrid-III lumbar spine in VertAc rig

Peak predicted transmitted force calculated using load cell cross-sections matched physical measurements (Denton Load Cell Model No. IF-221) to within 10% for all cases, with a Correlation and Analysis (CORA) score of 0.862 and 0.924 for the 1.2- and 2.4-m/s cases, respectively (Table 2). Traces of the transmitted force for both the FEM simulations and the MCW VertAc tests are shown in Fig. 3. Both the CORA scores and data traces indicate that there is a good correlation between the simulation and the experimental tests, validating the FEM.

Table 2 VertAc rig validation using Hybrid-III FEM; CORA scores

Peak velocity	L1 Force (+Z) CORA overall	L1 Force (+Z) CORA phase shift	L1 Force (+Z) CORA size	L1 Force (+Z) CORA progression	L1 Force (+Z) CORA corridor
1.2 m/s	0.862	0.945	0.968	0.833	0.828
2.4 m/s	0.924	1.000	0.855	0.932	0.917



Note: Force transmission of experiment compared to finite element analysis (FEA) at a) 1.2 m/s and b) 2.4 m/s.

Fig. 3 VertAc rig validation cases

2.2 Preliminary Material Optimization

To help inform the material selection for the Lumbar Spine Materials Demonstrators, a preliminary optimization of the compliant elements' material had to be performed. For this preliminary optimization, a Blatz-Ko constitutive model was calibrated to maximize agreement between transmitted force between the validated VertAc FEM and physical testing. Because of the lack of experimental characterization at the time, an additional damping term was added to the Blatz-Ko model, with an effective damping force proportional to nodal velocity at any given point. Preliminary BRCs were generated using experimental transmitted force traces (Denton Load Cell Model No. IF-221) from 3 PMHS lumbar spines, which were each impacted in the VertAc rig at 0.8, 1.2, and 2.4 m/s.

The optimization consisted of 10 simulations at each velocity, with the pucks' shear modulus varied from 1 to 15 MPa, and input accelerations defined using lower carriage accelerations from the PMHS experiments. The material giving the lowest average percent difference in peak transmitted force compared to preliminary BRCs at each input velocity was selected as the optimized material.

A shear modulus of 2.5 MPa, corresponding to a Shore A hardness of 64, was the result of the optimization, and was leveraged to inform material selection for subsequent materials characterization and WIAMan Lumbar Spine Materials Demonstrator fabrication. Optimized force transmission cases compared against PMHS corridors are shown in Fig. 4. CORA scores calculated using the default settings are shown in Table 3.

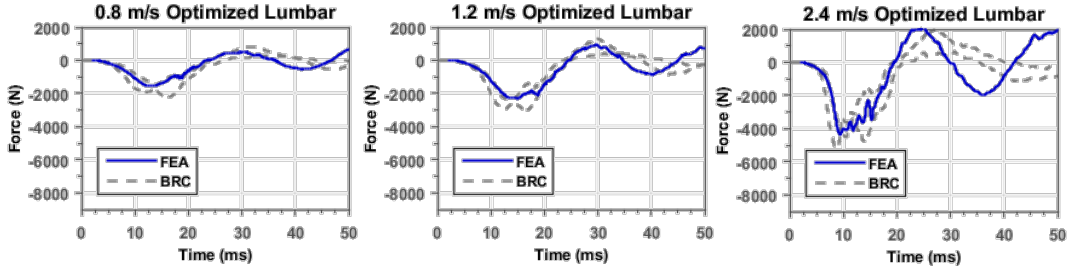
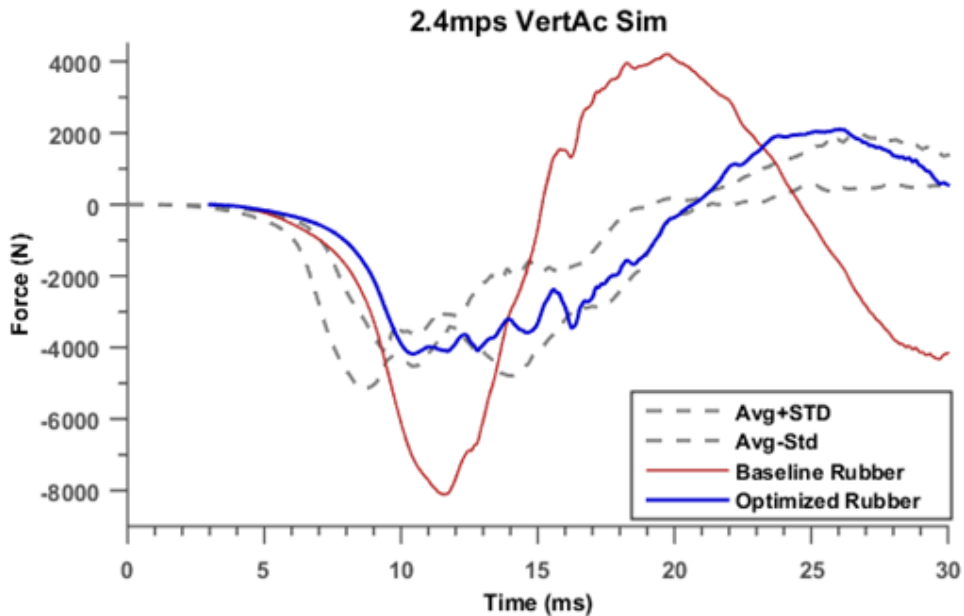


Fig. 4 Optimized ATD lumbar spine force transmission results

Table 3 Lumbar spine rubber optimization against L1 force BRCs; CORA scores

Peak velocity	L1 Force (+Z) CORA overall	L1 Force (+Z) CORA phase shift	L1 Force (+Z) CORA size	L1 Force (+Z) CORA progression	L1 Force (+Z) CORA corridor
0.8 m/s	0.748	0.867	0.581	0.924	0.672
1.2 m/s	0.827	1.000	0.672	0.911	0.781
2.4 m/s	0.738	1.000	0.882	0.676	0.667

The rubber specified in the Humanetics TDP was neoprene with a Shore A hardness of 75. The conclusion from the preliminary material optimization study was that the TDP-specified rubber showed a response that was stiffer than desired when compared to initial PMHS response corridors. Hence, this material represented an upper bound on the selection of materials for experimental test. Figure 5 shows plots of the TDP-specified rubber (Baseline) and the preliminarily optimized rubber against the preliminary BRC for a 2.4-m/s impact.



Note: Comparison of baseline TDP specified rubber, optimized Blatz-Ko rubber, and BRC.

Fig. 5 Comparison of force transmission predictions

3. Materials Characterization

3.1 Material Selection

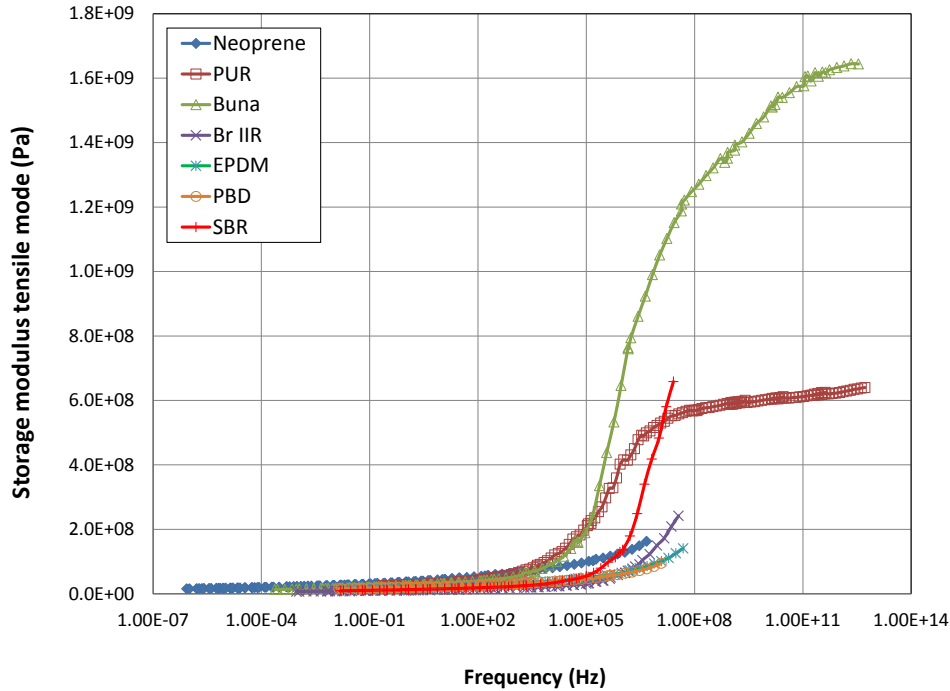
Seven rubber families were selected as candidates for the Lumbar Spine Materials Demonstrators based on mechanical damping, strain-rate sensitivity, tear resistance, and strain recovery. The 7 rubber families selected were as follows:

- Neoprene
- Polyurethane (PUR)
- Buna-N (nitrile butadiene rubber, NBR)
- Brominated butyl (Br IIR, also referred to in this report as BR)
- Ethylene propylene diene monomer (EPDM)
- Polybutadiene/natural rubber blend (PBD/NR)
- Styrene butadiene rubber (SBR)

Of these, neoprene, PUR, and Buna-N were purchased as stock materials from McMaster-Carr.

The other 4 materials (Br IIR, EPDM, PBD/NR, and SBR) were custom compounded by the Akron Rubber Development Laboratory (ARDL).

All 7 rubbers were tested via dynamic mechanical analysis (DMA) at temperatures from -90 to 100 °C and at frequencies ranging from 1 to 30 Hz. A strain sweep was performed for determining the linear viscoelastic range of the rubber prior to the DMA temperature sweep tests. After the test, the storage modulus data were processed using the time-temperature superposition principle using 20 °C as the reference point. Figure 6 shows the storage modulus as a function of frequency after the time-temperature superposition curve shift. The DMA master curves illustrate the rate dependence of the various rubber families by plotting storage modulus (elastic component of the complex modulus) as a function of oscillation frequency. Based on this graph, in the glass transition region (i.e., the region that shows the change in storage modulus [10^5 to 10^8 Hz]), EPDM and PBD/NR have the least amount of rate sensitivity.



Note: DMA master curves, illustrating the rate dependence of the various rubber families by plotting storage modulus (elastic component of the complex modulus) as a function of oscillation frequency.

Fig. 6 DMA master curves

Neoprene has comparable rate sensitivity to SBR and EPDM based on this analysis. However, neoprene was not selected for testing due to an “unstable” structure that develops upon mechanical deformation. Because of its unique molecular architecture, neoprene is known for its ability to crystallize upon cooling or mechanical straining (strain-induced crystallization). Even in the vulcanized state, neoprene still crystallizes. Traditional sulfur curing is not sufficient to prevent the structure from further crystallizing.

Table 4 shows data on mechanical damping (as indicated by $\tan \delta$ from DMA), strain recovery, and retardation time for all 7 rubbers. At similar Shore A hardness levels (around 70), these rubbers are different in many ways. PBD/NR and EPDM have the lowest glass transition temperature, which is a positive, as it ensures the 2 materials are in the rubbery region at ambient conditions.

Table 4 Thermal and thermomechanical results

Sample	TanD peak temp (°C)	TanD @ Tg	TanD @ 23 °C	Shore A measured	Recovery (%) after 200 s (100 s creep, 100 s recovery)	Retardation time (s)	TGA polymer weight (%)
Neoprene	-40	0.76	0.31	74	60	15	45
Buna	-21	0.74	0.24	76	62	17	55
Br IIR	-41	0.67	0.22	71	68	19	58
PBD	-55	0.59	0.18	77	70	16	58
EPDM	-44	0.59	0.18	76	62	20	55
SBR	-41	0.96	0.14	74	77	17	64
PUR	-17	0.54	0.08	75	71	19	95

Based on these analyses, PBD/NR and EPDM were selected for the fabrication of the Lumbar Spine Materials Demonstrators for testing at MCW. To cover a broad range of hardness, both rubbers were formulated at 60 and 75 Shore A hardness levels. In addition, PBD/NR was also formulated to a much softer version to determine the benefit of extra softness on the mechanical performance. Details on the rubber formulations for PBD/NR and EPDM are provided in Tables 5 and 6.

Table 5 Formulation details for PBD/NR

NR/PBD natural rubber and polybutadiene	75A	60A	45A	Details	Vendor
Ingredients:	phr	phr	phr
SMR CV60	50	50	50	Natural rubber with constant viscosity	Harwick standard
1207	50	50	50	high cis-1,4 polybutadiene	Goodyear
N330	75	30	5	carbon black	Akrochem
Sundex 790	2	2	2	aromatic processing oil	RE Caroll
Kadox 911-ZnO	5	5	5	react with stearic acid to Zn stearate	Harwick Standard
Stearic acid	2	2	2	see above	Harwick Standard
Agerite stalite	2	2	2	antioxidant	RT Vanderbilt
MBTS	1	1	1	accelerator-Benzothiazyl Disulfide	Harwick Standard
TMTD	0.1	0.1	0.1	accelerator-Tetramethylthiuram Disulfide)	Archochem
Sulfur	2.75	2.75	2.75	crosslinker	Lintech
Total	189.85	144.85	119.85

Table 6 Formulation details for EPDM

EPDM	75A	60A	Details	Vendor
Ingredients	phr	phr
Vistalon 2504	100.0	100.0	EPDM	RT Vanderbilt
N762	125.0	78.0	carbon black	Akrochem
Flexon 580	50.0	50.0	processing oil	RE Carroll
Kadox 911-ZnO	5.0	5.0	reach with stearic acid	Harwick Standard
Stearic acid	1.0	1.0	see above	Harwick Standard
TMTD	3.0	3.0	accelerator-Tetramethylthiuram disulfide	Harwick Standard
MBT	0.5	0.5	accelerator-(2-Mercaptobenzothiazole	Archochem
Sulfur	1.5	1.5	crosslinker	Lintech
Total	286.0	239

3.2 Material Characterization Testing

Rubber samples from 4 different families were selected for characterization. These included the 2 rubbers selected for the Lumbar Spine Materials Demonstrators (EPDM and PBD/NR blend), as well as 2 other rubbers (Br IIR and SBR) formulated by ARDL that had been tested previously (along with EPDM and PBD/NR) as tibia compliant elements in the JHU/APL lower leg demonstration unit. All of the rubbers were formulated to a Shore A hardness of 75A. In addition, EPDM was formulated to 60A and PBD/NR was formulated to 60A and 45A, for a total of 7 unique rubber sample types. All of the sample types were tested in both uniaxial compression and uniaxial tension to develop an idealized material response for the development of FEA material model parameters. Material response (stress) is characterized as a function of strain, strain rate, and loading mode (uniaxial tension versus uniaxial compression).

3.2.1 Compression Testing

Compression samples were prepared in a cylindrical geometry according to ASTM D575.² The samples had a nominal diameter of approximately 28.6 mm and a height of 12.5 mm, but each specimen was measured individually to get specific and accurate stress-strain conversions. The 7 materials were tested at 4 strain rates (2 samples per material with 2 repeats, resulting in 112 tests). An example test matrix for BR is shown in Table 7.

Table 7 Single material test matrix (butyl rubber) for compression

Sample type	Sample no.	Repeat no.	Rates (s ⁻¹)			
			0.01	1	10	50
Br IIR	1	1	x
Br IIR	1	2	x
Br IIR	2	1	x
Br IIR	2	2	x
Br IIR	1	1	...	x
Br IIR	1	2	...	x
Br IIR	2	1	...	x
Br IIR	2	2	...	x
Br IIR	1	1	x	...
Br IIR	1	2	x	...
Br IIR	2	1	x	...
Br IIR	2	2	x	...
Br IIR	1	1	x
Br IIR	1	2	x
Br IIR	2	1	x
Br IIR	2	2	x

Note: This matrix was completed for each of the 7 samples.

These strain rates included 0.01, 1, 10, and 50 strain per second. Each sample was taken to approximately 50% strain in compression. Each rate had different procedures to best account for the needed rate and duration of the test. The 0.01 s⁻¹ test was run on a screw-driven electromechanical load frame (MTS30/G). The samples were placed, centered, between 2 lubricated platens. This was done to create a uniaxial stress condition. The crosshead displacement was used for the strain measurement and the load data were collected with a 30-kN load cell (MTS No. 27.00110). The acquired data were sampled at 6.25 Hz and it included the channels of time, crosshead displacement, and load.

The 1, 10, and 50 s⁻¹ rate tests were run on a hydraulic high-rate Instron MTS (8821S) between 2 lubricated platens (Fig. 7). Strain data were determined from piston displacement, which was verified using a Vision Research Phantom v711 high-speed monochrome camera. The camera was used to track photo targets on the surface of the upper and lower platens at video frame rates of 2000, 4000, and 7500 Hz for the 1, 10, and 50 s⁻¹ rate tests, respectively, and had a resolution of approximately 3.9 pixels per mm. The load cell used in the 1, 10, and 50 s⁻¹ rate tests was a Dynacell 25 kN piezoresistive load cell (2527-101). The acquired data were sampled at 50 kHz and they included the channels of time, crosshead displacement, and load.

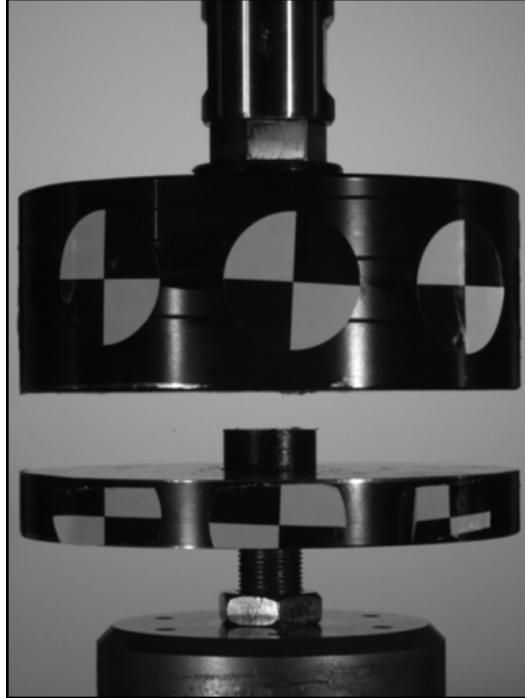


Fig. 7 Compression sample with lubricated platens

Nominal strain rates were targeted, but the actual strain rates were determined for each compression test, and the mean values are provided in Table 8.

Table 8 Average achieved strain rates for compression

Nominal strain rate (s ⁻¹)	Mean rate achieved (s ⁻¹)
0.01	0.01 ± 0.001
1	1.47 ± 0.078
10	16.79 ± 0.574
50	37.04 ± 1.84

Data reduction techniques were employed to gain idealized average response stress strain curves. All of the data traces analyzed were truncated to 30% strain in compression. The steps included 1) smoothing, 2) time shifting to onset of load, 3) strain shifting to align linear region of stress-strain curve, 4) interpolation to regularized strains, and 5) curve averaging. A 1-ms moving average filter was applied to the load and displacement data. The time shift was accomplished by an x-intercept method by finding the x-intercept of a line fit from the point on the curve corresponding to -200 and -800 N compression load. The strain was shifted in a load-strain curve in a similar x-intercept manner with the load values of -200 and -800 N. Interpolation was achieved by using a binning technique with bin widths of 0.1% strain. For repeat tests of a particular sample a slight reduction in stress for a given strain after the initial test was observed. This is described as the Mullins

Effect. This known material response phenomenon was used to justify omitting the first repeat of each sample from the final average curves. Average curves were created from the second loading test across all samples for a given material at the same rate.

3.2.2 Tension Testing

Although the primary loading mode of the lumbar spine is compressive, the compliant elements of the spine are expected to see significant tensile stresses due to rebounding (unloading) of the initial compressive loading pulse. Tension testing also allows for the characterization of higher strain response than is possible in compression, as well as the determination of failure (rupture) stress and strain.

Tension samples were prepared in a dog bone geometry (“Die C”) according to ASTM D412.³ The gauge width and thickness were approximately 6.35 and 2 mm, respectively, and were measured for each specimen to get specific and accurate stress-strain conversions. The 7 materials were tested at 4 rates (2 samples per material, equating to 56 tests). An example test matrix is shown in Table 9.

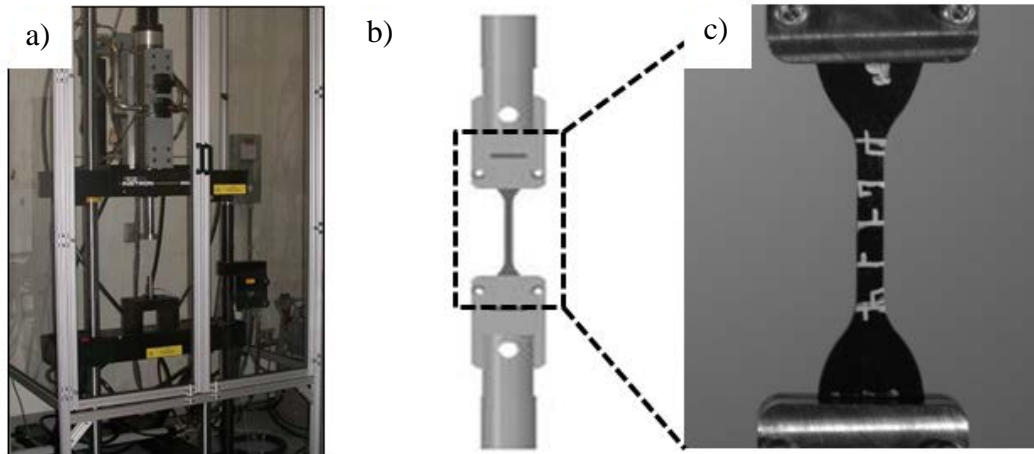
Table 9 Single material test matrix (butyl rubber) for tension

Sample type	Sample no.	Repeat no.	Rates(s ⁻¹)			
			0.01	1	10	50
Br IIR	1	1	x
Br IIR	2	1	x
Br IIR	1	1	...	x
Br IIR	2	1	...	x
Br IIR	1	1	x	...
Br IIR	2	1	x	...
Br IIR	1	1	x
Br IIR	2	1	x

Note: This matrix was completed for each of the 7 samples.

These strain rates included 0.01, 1, 10, and 50 strains per second (s⁻¹). Each sample was taken to failure. Each rate had different procedures to best account for the needed rate and duration of the test. The 0.01 s⁻¹ test was run on a screw-driven electromechanical load frame (MTS30/G). The samples were placed in a self-tightening clamp fixture with a sample clamped length of 80 mm. The strain data were gathered by using a laser extensometer and the load was collected with a 2.5-kN load cell (MTS No. 380198). The acquired data was sampled at 6.25 Hz and it included the channels of time, crosshead displacement, extensometer displacement, and load.

The 1 and 10 s⁻¹ rate tests were run on a hydraulic high-rate Instron MTS (8821S), placed in a custom-designed tension fixture (Fig. 8).



Note: a) High-rate Instron MTS machine (8821S), b) custom tension clamp fixture CAD, and c) tension sample in custom tension fixture.

Fig. 8 Custom fixture for high-rate testing

Strain data were determined from 1-D Digital Image Correlation via a Vision Research Phantom v711 high-speed monochrome camera. The camera was used to track photo targets on the surface of the sample at 2000 and 4000 Hz for the 1 and 10 s^{-1} rate tests, respectively, and had a resolution of approximately 3.9 pixels per mm. The strain values were processed from the tracked markers on the surface (template matching image processing algorithm in PCC software), and the relative distance between the furthest targets on the gauge region were used to calculate strain. The load cell used in the 1 and 10 s^{-1} rate tests was a Dynacell 1 kN piezoresistive load cell (2527-130). The acquired data were sampled at 50 kHz, and it included the channels of time, crosshead displacement, and load.

Initially, the 50 s^{-1} rate test followed the same procedure as the 1 and 10 s^{-1} rate tests except the high-speed imaging was acquired at 7500 Hz and had a resolution of approximately 5.3 pixels per mm. The tensile clamp fixture included a “slack” fixture. The slack fixture was a slotted hole where the piston would not engage the sample until it had reached the optimal velocity. The slot was around 5 inches in length and the ramp up travel was approximately 4 inches. The slack fixture resulted in optimal velocities but also unwanted harmonic material response on initial impact. To mitigate the noise, the samples were shorted to accommodate an 18-mm clamped height. This allowed for slower piston velocities to achieve desired strain rates. Visual markers were placed closer together and markers in the center of the gauge region and were used for strain measurements to avoid edge effects (Fig. 9).



Fig. 9 Shortened test sample for high-rate (50 s-1) tension testing

The acquired data were sampled at 50 kHz and it included the channels of time, crosshead displacement, and extensometer displacement and load. Nominal strain rates were targeted, but the actual strain rates were determined for each tension test, and the mean values are provided in Table 10, the average achieved strain rates for tension.

Table 10 Average achieved strain rates for tension

Nominal strain rate (s ⁻¹)	Mean rate achieved (s ⁻¹)
0.01	0.01 ± 0.001
1	1.47 ± 0.078
10	16.79 ± 0.574
50	37.04 ± 1.84

Data reduction techniques were employed to gain idealized average response stress strain curves. All of the data traces analyzed were truncated to 120% strain in tension. As with the compression test data reduction, the steps included 1) smoothing, 2) time shifting to onset of load, 3) strain shifting to align linear region of stress-strain curve, 4) interpolation to regularized strains, and 5) curve averaging. A 1-ms moving average filter was applied to the load and displacement data. The time shift was accomplished by an x-intercept methods by finding the x-intercept

of a line fit from the point on the curve corresponding to 10 and 20 N tensile load. The strain was shifted in the stress-strain curve in a similar x-intercept manner with the stress values of the onset of the test and 50 Pa greater than that onset (Fig. 10).

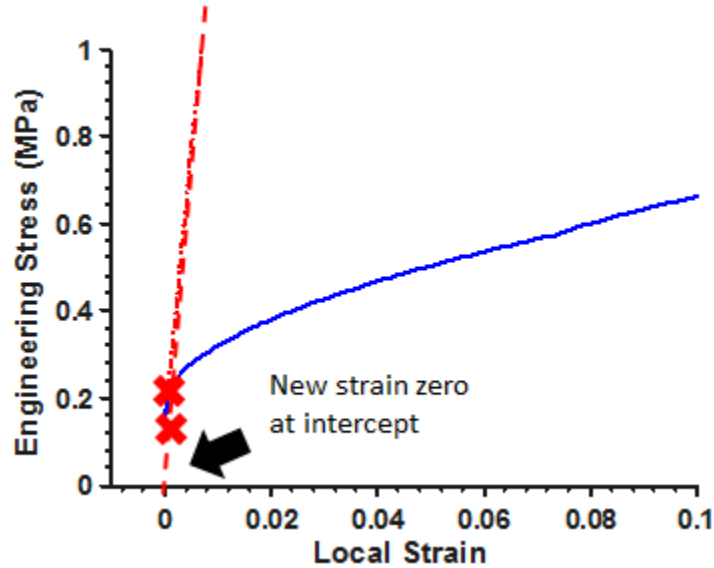


Fig. 10 X-intercept method with stress strain curve to achieve strain shift

Interpolation was achieved by using a binning technique with bin widths of 0.1% strain. Average curves were created from 2 tests using the same material at the same rate.

3.2.3 Combined Results

Results were combined at the zero-stress, zero-strain conditions set by the binning technique. This resulted in combined average curves going from 30% compression to 120% tension. Individual rates of the combined tests were noted in a spreadsheet but were counted as similar nominal rates. Results for each test were output to a spreadsheet, as combined average curves at regularized strains. Figure 11 shows the response of different materials at the nominal rates. These results were delivered to the modeling team, resulting in one characteristic curve (spanning 30% compression to 120% tension) for each material at a given rate. These curves were then used as input to the material models that were used in the FEM simulations.

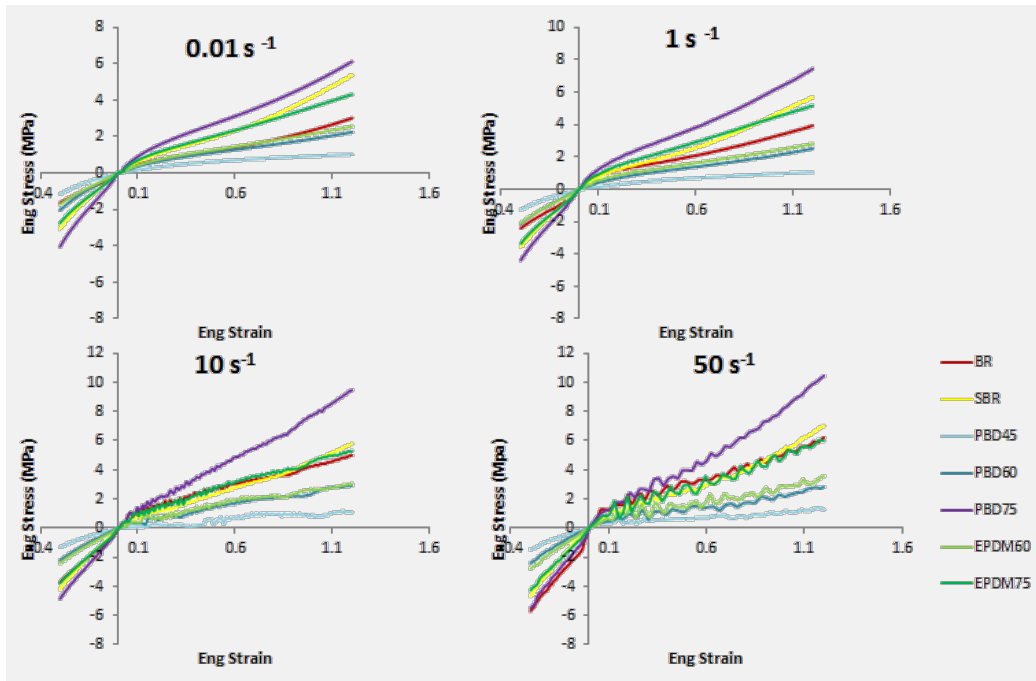


Fig. 11 Combined average stress strain curves

4. Fabrication Efforts

4.1 TDP Design

The WIAMan lumbar spine, Humanetics part number 130-4120, is an assembly of aluminum plates, aluminum discs, and compliant, molded rubber pucks. The final assembly is fabricated using a complex mold that will have 3 individual cavities to fill with rubber that are separated by the aluminum discs. Prior to injecting the rubber, the aluminum parts are coated with a Chemlok brand primer and adhesive. As the rubber crosslinks within the mold, the rubber will adhere to the Chemlok adhesive, forming a single component when it is removed from the mold.

4.2 Lumbar Spine Assembly

The components and materials specified in the TDP are shown in Fig. 12. Table 11 lists each component, its material, and any additional notes of significance about the individual parts.

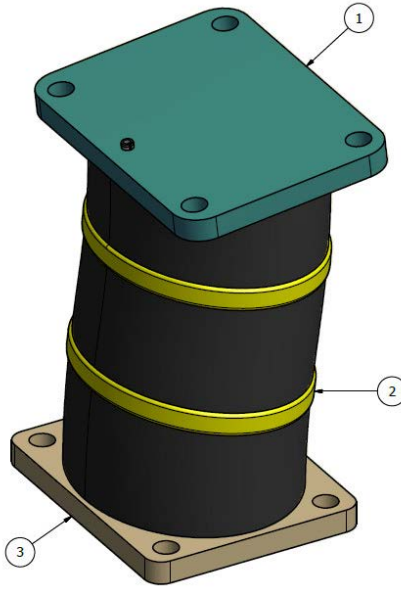


Fig. 12 Lumbar spine per Humanetics drawing 130-4120

Table 11 Materials specified for lumbar spine components in TDP

Component	Material	Additional specification
Top plate	7075-T6 Al	Clear anodize
Lumbar disc	7075-T6 Al	Clear anodize
Bottom plate	7075-T6 Al	Clear anodize
Compliant elements	Black neoprene	75 ± 5 Shore “A” hardness

The Lumbar Spine Materials Demonstrators were fabricated at JHU/APL and deviated from the TDP in several ways. Because of an aggressive schedule, there was not enough time to fabricate the complicated mold that would allow for building the spine as a molded-in-place assembly, per the TDP. Instead, each component was fabricated individually and then bonded together using Hysol EA9309.3NA epoxy. The layers of adhesive were approximately 0.005-inches thick and therefore added height to the final assembly. This was deemed acceptable because the molding tolerance for height was 1% of over 5 inches and it was not expected that 6 adhesive layers would add more than 0.05 inch of height. Additional adhesive testing details can be found in Section 1.2.2.

Another deviation from the TDP was the material choices for the compliant elements. Based on previous knowledge gained from WIAMan tibia compliant element testing, 2 material families were chosen for testing of the lumbar spine. EPDM and PBD/NR were chosen due to their strain-hardening coefficients and rate sensitivity. Six spines were fabricated using these 2 materials with a range of hardness from 45 to 75 Shore A. The 6 Lumbar Spine Materials Demonstrators that were fabricated are listed as follows:

- 1) PBD/NR 45A
- 2) PBD/NR 60A
- 3) PBD/NR 75A
- 4) EPDM 60A
- 5) EPDM 75A (1)
- 6) EPDM 75A (2): Two spines with the same material were tested to look at component-to-component repeatability of the test setup and to test the strength of the epoxy bond.

The final deviation from the TDP lies within the process to prepare the surfaces of each individual component for bonding. The assembly method used for this study involved curing and bonding the rubber in separate steps, requiring additional surface preparation to achieve successful bonding. Details of this surface preparation are provided in Section 4.2.1.

4.2.1 Assembly Method

The Humanetics TDP specifies that the lumbar spine compliant elements be “molded-in-place”. That process requires a vulcanizing rubber adhesive be applied to the metal surfaces. The uncured rubber is bonded to the metal in the mold during the curing process at elevated temperature and pressure. This process results in a strong bond that is typically stronger than the rubber itself. Tests of the adhesive bond strength were also completed to compare the bonding of the postcured epoxy adhesive to the molded-in-place vulcanized bonding. Details of the adhesive tests are provided in Section 4.2.2.

The 7075-T6 aluminum end plates and aluminum discs were machined and clear anodized per TDP specifications; however, additional processes were necessary to prepare these components for bonding to the EPDM and PBD/NR pucks. Only the surfaces that would be exposed after bonding were anodized. To prepare the other surfaces for adhesive application, processes developed by the aerospace industry and documented by internal JHU/APL specifications were used. The following processes cover the etching and priming techniques that create the ideal bonding surface on aluminum components:

- Q53-576, “Surface Preparation of Aluminum Alloys Prior to Adhesive Bonding”⁴
- QF3-502, “Application of BR-127 Primer”⁵
- Q53-667, “Fabrication and Acceptance of Adhesive Bonded Assemblies”⁶

While the aluminum components were being machined and prepared for assembly, the compliant elements were being individually molded at ARDL. All rubbers were cured using a combination of sulfur and hydroxides. To tune the final hardness value, different levels of carbon black were used (higher hardness is achieved via higher carbon black content). An isopropyl alcohol cleaning followed by abrasive roughening and then a second isopropyl alcohol cleaning were used to prepare the rubber surfaces for bonding.

An assembly rig was used to securely hold each component of the lumbar spine so that pressure could be applied during epoxy curing without causing misalignment. It was necessary that the alignment fixture clamp around each component but not block access to the bonding seams because they were continually cleaned to remove excess epoxy that was squeezed out during the initial curing stage. To meet the demands of the schedule, the assembly rig was 3-D printed in black acrylonitrile butadiene styrene (ABS) using a fused deposition modeling machine.

The assembly process began once the machined components were prepared for bonding. The compliant elements were received from ARDL and cleaned, and the alignment fixture was printed and assembled. The lumbar spine assembly process consisted of carefully stacking the components, one at a time, in the alignment fixture and tightening down the adjustable clamps (Fig. 13). The clamps are individually tightened to align the compliant pucks using the matching primed face on the aluminum components as an alignment guide. After one component was secured in place, the next was prepared with a layer of epoxy and placed in position within the fixture. Once all of the components were in place, the top of the rig was staked in place using extra-strength tape for additional support and a 5-lbf weight was placed on top. The added pressure from the weight helped the curing process by squeezing out excess epoxy from each layer, which was continually cleaned for the first few minutes of the curing process.

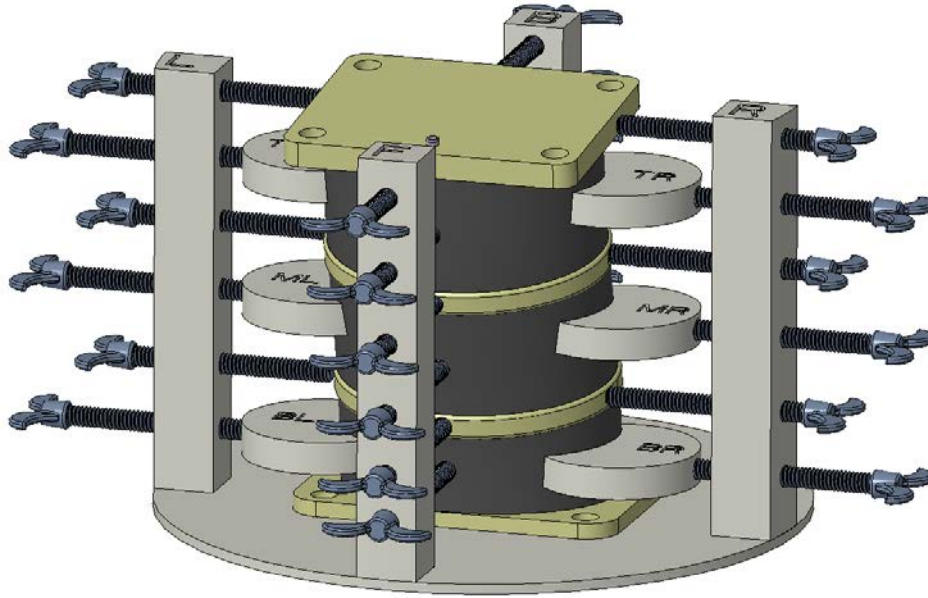


Fig. 13 Lumbar spine assembly in alignment fixture

4.2.2 Adhesive Testing

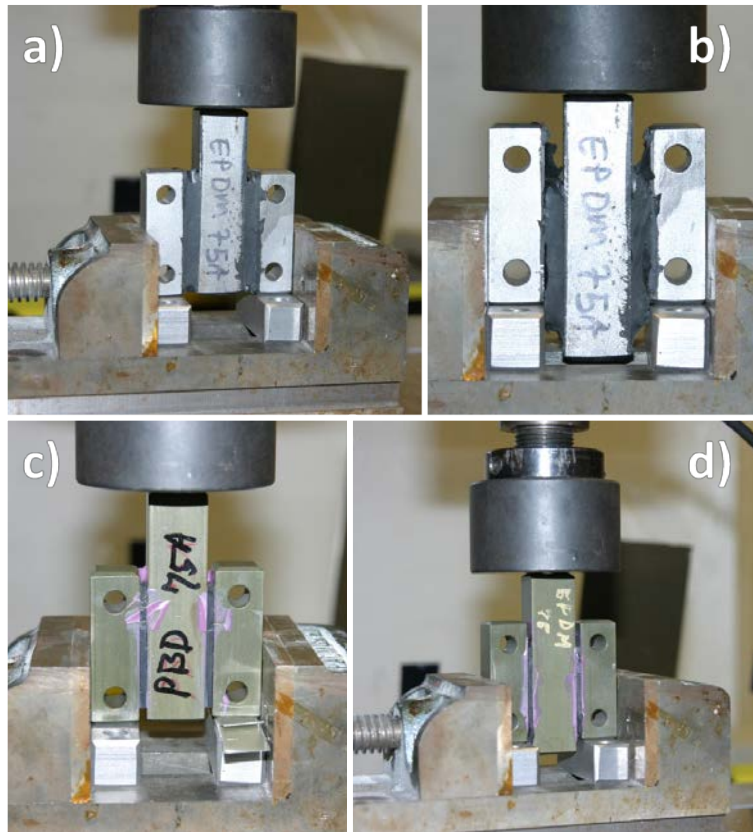
Testing of the adhesive bond strength was conducted using a double-lap shear coupon configuration prepared according to ASTM D5992.⁷ Sample coupons of EPDM and PBD/NR rubber at a nominal hardness of Shore 75A were prepared by ARDL and JHU/APL. The primary objective of the test was to provide a direct comparison between the shear strength of adhesive bonds between metal and EPDM and PBD/NR rubbers using 2 different approaches: bonding during rubber molding (“molded-in-place”) using a vulcanizing adhesive and bonding the rubber components after curing with an epoxy adhesive.

Three samples of both rubbers were bonded during the curing process at ARDL using Chemlok 205 primer and Chemlok 220 adhesive (LORD Corp). These samples represent bond strength characteristic of rubber components that are “bonded-in-place” with metallic components in the rubber casting mold, which is the nominal process for bonding the ATD lumbar spine per the current TDP.

Three samples using fully cured rubbers were prepared at JHU/APL using Hysol 9309.3NA epoxy and a JHU/APL standard procedure for cleaning and priming the surfaces prior to adhesive bonding. The coupons represent the bond strength characteristic of the lumbar spine elements fabricated by JHU/APL for testing at MCW. The metallic components of the lap shear coupons were steel, so JHU/APL Standard Q53-599,⁸ “Surface Preparation of Low Carbon Steel Alloys Prior to Adhesive Bonding” was followed for etching the samples. Then the samples were primed with BR-127 per QF3-502,⁵ “Application of BR-127 Primer.” The rubber

components for the coupons were cut from 2-mm-thick sheets (provided by ARDL), cleaned with isopropyl alcohol (IPA), and abraded using 320-grit sand paper. The rubber was then re-cleaned with IPA and allowed to air dry. After mixing the adhesive, it was applied to the metal surfaces and the samples were sandwiched and clamped together to form the double-lap shear specimens. Excess adhesive was wiped off and the samples were allowed to cure overnight before handling. Full cure was achieved at room temperature after 5 days.

The double-lap shear coupons were tested in compression on an electromechanical MTS load frame. The fixturing arrangement is shown in Fig. 14. The coupon was supported in a machinist's vice that maintains parallelism of the sides of the coupon and prevents lateral expansion. The vice merely constrained the coupon; it was not used to apply a lateral compression prior to shear testing. The sides of the coupon rest on blocks at the bottom of the vice jaw to allow for travel of the center post when pushed downward by the upper platen of the MTS load frame. The upper platen is rigidly connected to a 500-lbf load cell for recording load versus crosshead displacement during the test.



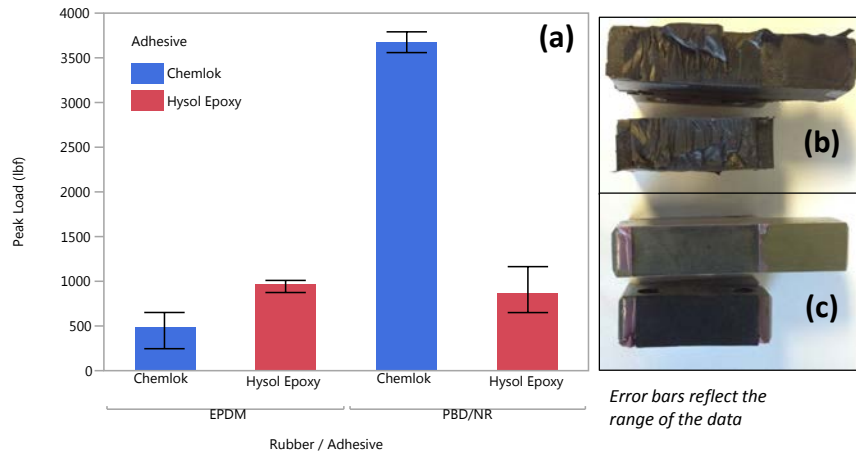
Note: a) Bonded-in-place EPDM before test, b) EPDM bonded-in-place after test, c) EPDM epoxy-bonded before testing, and d) EPDM epoxy-bonded after test

Fig. 14 Double-lap shear coupons before and after testing

Figure 14 shows that the rubber layers in the Chemlok samples (Figs. 14a and 14b) were thicker than the rubber layers in the epoxy samples (Figs. 14c and 14d). Although the difference in thickness was large (2 vs. 5 mm), the impact of this difference on the shear strength of the adhesive bonds was expected to be low. The primary difference in response due to the difference in rubber thickness was the amount of displacement required to achieve equivalent shear strains in the 2 coupon types, but capturing shear strain capability of the rubber was not an objective for this test. However, the thickness of the rubber was considered when establishing a constant shear strain rate for all coupons (0.01 s^{-1}).

Some of the epoxy-bond coupons had offset side posts, and in those cases shims (Fig. 14c), were used to minimize uneven loading of the 2 sides of the double-lap shear coupon. Although the Chemlok coupons were not offset, their side posts were slightly off-parallel. Neither of these 2 coupon irregularities significantly impacted the test results.

The results from the lap shear testing are summarized in Fig. 15. The peak loads (directly proportional to the peak shear stress) are plotted for each sample type, grouped by rubber family (EPDM or PBD/NR) and bond type (Chemlok or Hysol Epoxy). The results are difficult to interpret without taking into consideration the mode of failure for each sample type. Figure 15 also shows characteristic failure surfaces for b) the Chemlok (molded-in-place) samples and c) the epoxy-bonded samples. All of the Chemlok samples failed cohesively within the rubber; there was no adhesive failure. In contrast, all of the rubber samples bonded with epoxy failed adhesively at the epoxy to rubber interface.

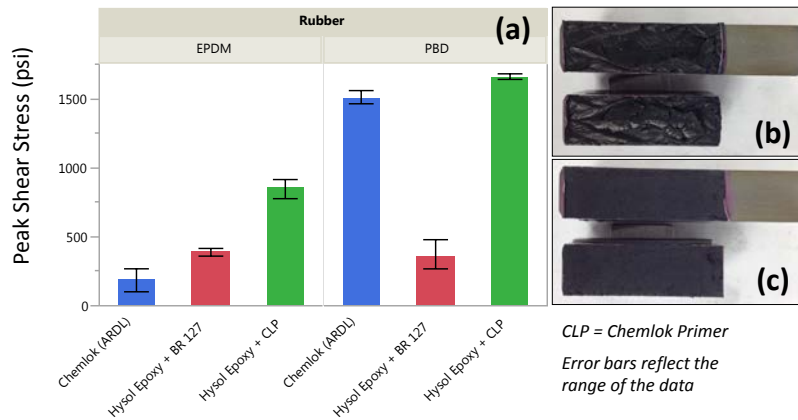


Note: a) Comparison of peak load from the lap shear coupons. Because the shear areas are equal for all the coupons tested, the comparison of peak loads correlates directly with peak shear stresses. b) Cohesive failure of the rubber was observed for all Chemlok (molded-in-place) coupons, while c) adhesive failure was always observed at the interface between the epoxy and rubber.

Fig. 15 Initial lap-shear testing results

For EPDM, the rubber used in the Chemlok samples had a lower shear strength than the epoxy bond. This implies that the rubber sheets used to make the epoxy-bonded coupons had higher shear strength than the rubber in the molded Chemlok coupons, which points to a difference in the curing of the rubber in these 2 coupon types. A possible explanation is that the EPDM rubber in the molded Chemlok coupons was not sufficiently cured (cross-linked). Therefore, a direct comparison of the Chemlok and epoxy-bond strengths cannot be made from the EPDM results.

For PBD/NR, the failure of the Chemlok coupons was also cohesive within the rubber (Figs. 16b and 16c are from PBD/NR coupons), but the shear strength of the rubber far exceeded the bond strength of the epoxy. Therefore, it could be conclusively stated that the bond strength of the Chemlok in-mold bonding process was significantly higher than that of the epoxy bonds (for PBD/NR, at least). The bond strength of Hysol 9309.3NA epoxy to EPDM and PBD/NR was roughly equivalent.



Note: a) Peak shear stress for EPDM (left) and PBD/NR coupons (right). Cohesive failure of the rubber was observed for both the b) PBD/NR and c) EPDM coupons bonded using Hysol 9309.3NA epoxy and Chemlok 7701 primer.

Fig. 16 Additional lap-shear testing results

After the lumbar spine assemblies were completed, new information was received about a primer (Chemlok 7701) designed for improving the adhesion of epoxy to fully cured vulcanized rubbers. A new set of lap shear coupons was made from the same 2-mm-thick sheets of Shore 75A EPDM and PBD/NR using the new primer and Hysol 9309.3NA epoxy. It is also suspected that the mechanical abrasion of the rubber surfaces prior to bonding was more thorough than what had been done for the earlier coupons. The new lap shear results are shown in Fig. 16. These results suggest that rubber surfaces bonded with epoxy and a suitable primer can have shear strengths that are functionally equivalent to those made using a molded-in-place process. Therefore, it should be possible to produce lumbar spine test components in the future that can be tested over relevant loading ranges (e.g., for

purposes of material selection, design optimization, and strength of design evaluation) without requiring the use of a full lumbar spine mold. This would be especially useful for testing changes to the lumbar spine geometry that would require changes to the mold.

4.3 VertAc Rig Interface and Mass Compensation

Before testing the lumbar spine assemblies, several extra components were required. To interface with the VertAc rig at MCW, interface blocks were fabricated to mount on either end of the spines. These can be seen in Fig. 17.

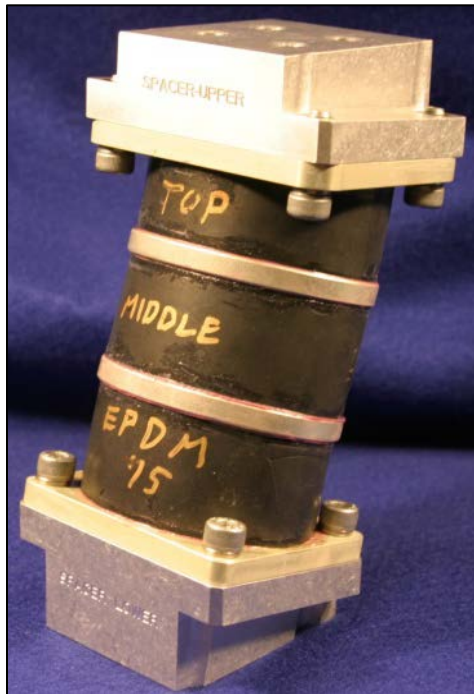


Fig. 17 Lumbar spine with VertAc rig interface blocks

Ballast plates were also fabricated from steel to add weight to the lumbar spines. The added weight accounted for the difference between the fabricated materials demonstrator lumbar spine assemblies and the average measured masses of the lumbar spines used in PMHS testing. The average mass of the lumbar spines used in the PMHS testing was 1.623 kg. The average mass of the PMHS upper potting and mounting block was 1.29 kg and the average mass of the PMHS lower potting and mounting block was 1.25 kg. Each of the materials demonstrator lumbar spines had slightly different masses depending on the hardness of the compliant material used, which meant that the ballast plates needed to be different for each of the different hardness spines. All of the materials demonstrator lumbar spines had masses that were less than the average mass from the PMHS testing. Knowing the materials demonstrator lumbar spine masses, the mass of the upper and lower

interface blocks, and the average masses of the PMHS components, it was possible to calculate the additional masses required to make each materials demonstrator spine assembly equivalent in mass to the PMHS average mass. Equations 1 and 2 were used to determine the required masses for the ballast plates for each materials demonstrator lumbar spine assembly. The results are provided in Table 12.

$$m_{UBP} = m_{UP} - m_{UIB} + \frac{m_{PMHS} - m_{MD}}{2} \quad (1)$$

$$m_{LBP} = m_{LP} - m_{LIB} + \frac{m_{PMHS} - m_{MD}}{2} \quad (2)$$

Table 12 Ballast plate mass comparison

Materials demonstrator components	PBD45A	PBD 60A	PBD 75A	EPDM 60A	EPDM 75A	PMHS Avg.	PMHS sample components
Upper interface block mass (m_{UIB})	0.625	0.625	0.625	0.625	0.625	1.290	Upper potting and mounting block mass (m_{UP})
Upper ballast plate mass (m_{UBP})	0.955	0.921	0.894	0.922	0.897		
Materials demonstrator lumbar spine mass (m_{MD})	1.043	1.112	1.166	1.110	1.160	1.623	PMHS lumbar spine mass (m_{PMHS})
Lower ballast plate mass (m_{LBP})	0.915	0.881	0.854	0.882	0.857	1.250	Lower potting and mounting block mass (m_{LP})
Lower interface block mass (m_{LIB})	0.625	0.625	0.625	0.625	0.625		
Total mass	4.163	4.163	4.163	4.163	4.163	4.163	...

Note: All masses are in kg.

5. Materials Demonstrator Testing

5.1 VertAc Overview

Lumbar spine PMHS testing that was used to generate the WIAMan lumbar spine BRCs was performed at MCW using one of MCW's 2 VertAc test machines. Each VertAc consists of 2 vertical tracks and a pivot arm. The first vertical track is used to guide the drop weight while it falls to ensure that it will hit the pivot arm. The second track has 2 carriages attached to it, one of which attaches to the bottom of the equipment under test (EUT), and the other of which attaches to the top of the EUT. A photograph of a WIAMan lumbar spine materials demonstrator mounted in the VertAc is provided in Fig. 18.

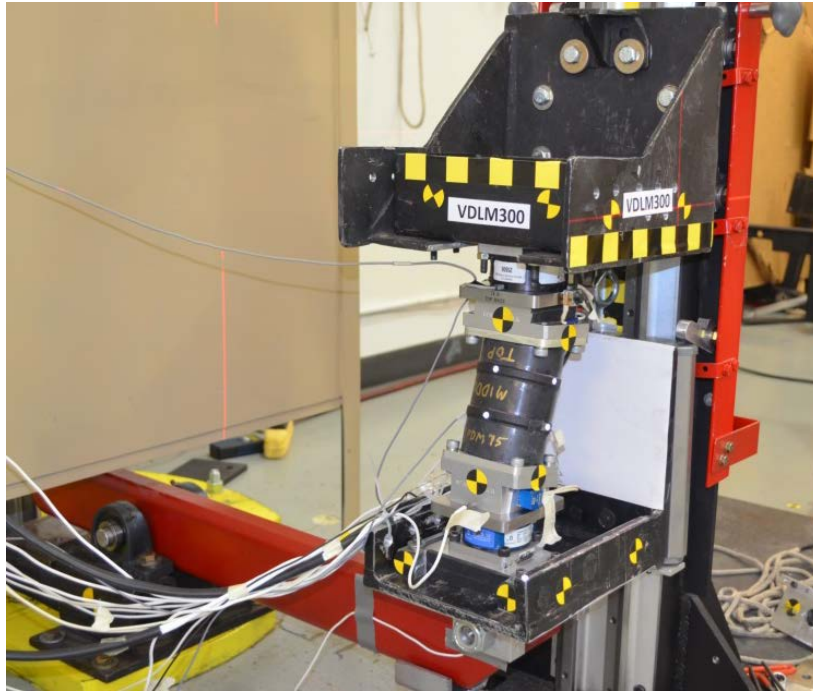


Fig. 18 Lumbar spine materials demonstrator mounted in VertAc rig

When a hit is conducted with the VertAc, the drop weight is lifted to a specified height on the first track and then released. The drop weight lands on one end of the pivot arm and forces the opposite end of the pivot arm to rise and impact the bottom of the lower carriage that is attached to the second track. The impact load is then transferred up into the lower carriage, EUT, and upper carriage. As the carriages rise up the track due to the impact, locking blocks fold out beneath the lower carriage to catch the carriages and EUT before they have a chance to fall back down to the pivot arm, potentially causing damage to the EUT or the VertAc.

For the Lumbar Spine Materials Demonstrator effort, the VertAc was used in an identical manner to that of the PMHS testing that was used to generate the lumbar spine BRCs. A detailed test plan was developed by JHU/APL for the Lumbar Spine Materials Demonstrator testing,⁹ using the PMHS setup and procedures as a guide. MCW participated in the review and approval of this test plan. The test plan defined the impact speeds that were to be used during the testing and how the VertAc carriages were to be instrumented with various sensors. These sensors and their setup will be discussed in detail in Section 5.3.

5.2 VertAc Test Method

Prior to testing all of the Lumbar Spine Materials Demonstrators, a pretest was conducted with the second EPDM 75A spine. The purpose of this pretest was to ensure that the epoxy adhesive used to assemble the lumbar spines would withstand

the impact loading of the planned tests. During this pretest, the spine was subjected to 6 impacts that were identical to those used to generate the BRCs, per the test plan (Table 13). The spine was hit twice at each impact speed. The spine was examined after each impact for damage and was found to have successfully survived these impacts with no observed damage.

Fig. 19 VertAc pretest matrix

Lumbar spine material	Hit no. 1 speed	Hit no. 2 speed	Hit no. 3 speed	Hit no. 4 speed	Hit no. 5 speed	Hit no. 6 speed
EPDM, 75A	0.8 m/s	0.8 m/s	1.2 m/s	1.2 m/s	2.4 m/s	2.4 m/s

Having survived these planned impacts, it was decided to hit the spine a seventh time at a higher speed to test the strength the spine’s survivability beyond the BRC requirements. The spine was hit at an impact speed of approximately 6 m/s for the seventh impact. During this high-speed impact, one of the rubber components did separate from one of the aluminum plates. The failure occurred at the interface between the epoxy adhesive and the rubber component. This was the expected mode of failure based on the lap shear testing. However, since the pretest spine survived all hits at the BRC speeds, it was decided to proceed with testing the rest of the lumbar spines.

Five lumbar spine assemblies were used in this test (in addition to the pretest spine), and each spine was hit several times at varying speeds, per the test plan. The minimum number of hits for each spine was specified to be 8, with each spine being hit at least twice at each of 4 different speeds. The 4 speeds of interest were 0.8, 1.2, 1.8, and 2.4 m/s. Three of these speeds corresponded to the speeds used to generate the BRCs (0.8, 1.2, and 2.4 m/s). The fourth speed (1.8 m/s) was to be used as a blind comparison to the simulation output. The test matrix for the lumbar spine testing at MCW is provided in Table 13.

Table 13 VertAc test matrix

Lumbar spine material	Hit no. 1 speed (m/s)	Hit no. 2 speed (m/s)	Hit no. 3 speed (m/s)	Hit no. 4 speed (m/s)	Hit no. 5 speed (m/s)	Hit no. 6 speed (m/s)	Hit no. 7 speed (m/s)	Hit no. 8 speed (m/s)
EPDM, 60A	0.8	0.8	1.2	1.2	2.4	2.4	1.8	1.8
EPDM, 75A	0.8	0.8	1.2	1.2	2.4	2.4	1.8	1.8
PBD, 45A	0.8	0.8	1.2	1.2	2.4	2.4	1.8	1.8
PBD, 60A	0.8	0.8	1.2	1.2	2.4	2.4	1.8	1.8
PBD, 75A	0.8	0.8	1.2	1.2	2.4	2.4	1.8	1.8

A minimum of 30 min between each impact was maintained throughout the testing to ensure there was adequate time for the compliant components to return to their original state. After each impact the lumbar spines were examined for any sign of damage.

5.3 VertAc Test Instrumentation

Various data were recorded during each impact. The lumbar spine and VertAc carriages were instrumented with sensors as shown in Fig. 20. The load cells produced force data in all 3 axes and moment data about all 3 axes. The angular-rate sensors produced angular-rate data in all 3 axes. Lateral and frontal high-speed video was also recorded for each hit. Load cell, accelerometer, and angular rate sensor data was recorded in Tab Separated Values format (the same format used for PMHS data). All data sets were time synced.

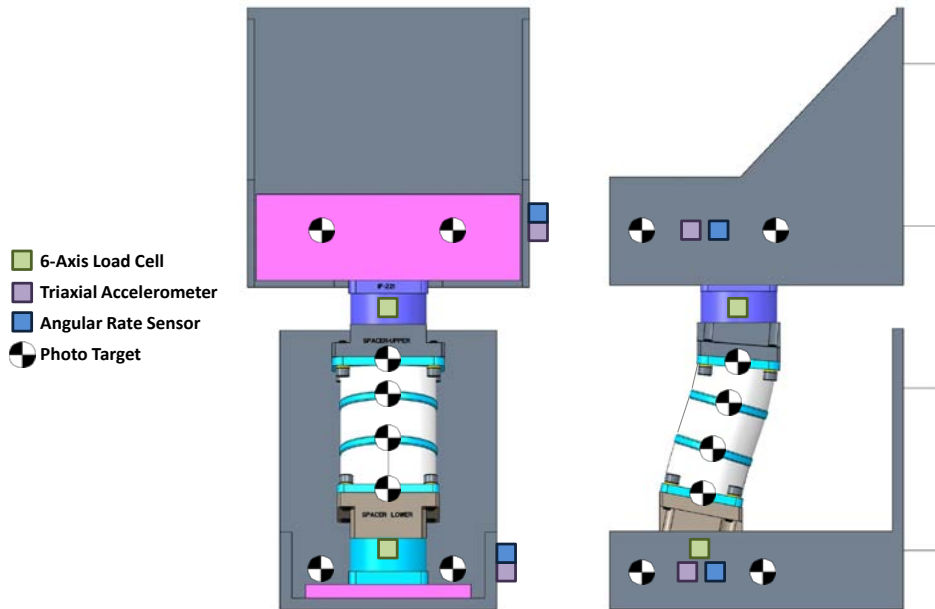


Fig. 20 VertAc rig instrumentation

All testing was performed in the same manner as that used for the PMHS testing of the lumbar spine that was previously conducted at MCW. The sampling rate for the load cells, accelerometers, and angular rate sensors was 100 kHz. A list of the data channels used is provided in Table 14.

Table 14 MCW testing data channels

Channel	Description	Symbol
1	Upper load cell x force	F_{xU}
2	Upper load cell y force	F_{yU}
3	Upper load cell z force	F_{zU}
4	Upper load cell moment about x	M_{xU}
5	Upper load cell moment about y	M_{yU}
6	Upper load cell moment about z	M_{zU}
7	Lower load cell x force	F_{xL}
8	Lower load cell y force	F_{yL}
9	Lower load cell z force	F_{zL}
10	Lower load cell moment about x	M_{xL}
11	Lower load cell moment about y	M_{yL}
12	Lower load cell moment about z	M_{zL}
13	Upper carriage x acceleration	a_{xU}
14	Upper carriage y acceleration	a_{yU}
15	Upper carriage z acceleration	a_{zU}
16	Lower carriage x acceleration	a_{xL}
17	Lower carriage y acceleration	a_{yL}
18	Lower carriage z acceleration	a_{zL}
19	Upper carriage angular rate about x	ω_{xU}
20	Upper carriage angular rate about y	ω_{yU}
21	Upper carriage angular rate about z	ω_{zU}
22	Lower carriage angular rate about x	ω_{xL}
23	Lower carriage angular rate about y	ω_{yL}
24	Lower carriage angular rate about z	ω_{zL}

The data recording pre/post triggers were -100 ms and $+1000$ ms, respectively. High-speed video was recorded at a frame rate of 5000 fps. Time stamps were included in the video recordings. Photographs were also taken at each phase of the test, including setup, before each impact, and after each impact.

5.4 VertAc Test Results

The Lumbar Spine Materials Demonstrators survived all of the planned impacts with one exception. The PBD/NR 45A spine suffered a bond failure during the first 2.4-m/s hit. The data for the compression phase of the response was still valid, but during the tension phase of the response, the bond between one of the rubber pucks and the epoxy adhesive failed. The second 2.4-m/s hit was not able to be completed after this failure.

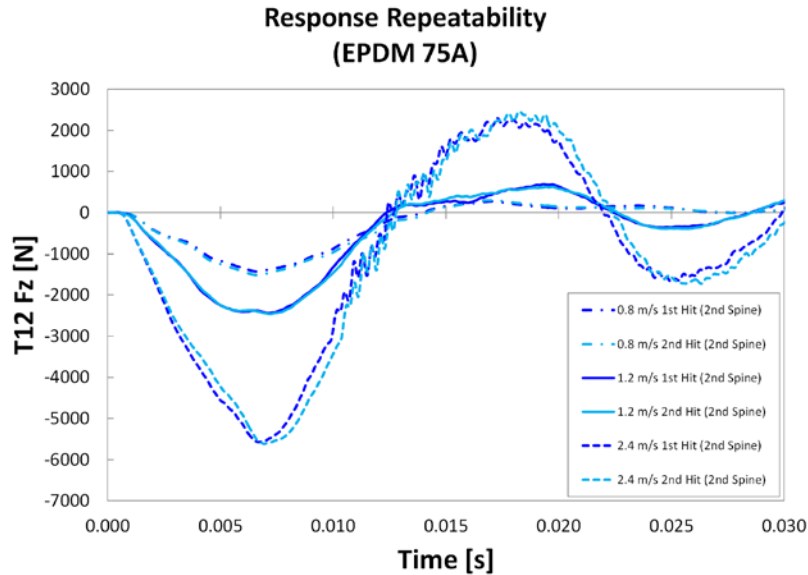
In addition to the planned 6 hits for each Lumbar Spine Materials Demonstrator, hits at higher speeds were conducted to further test the strength of the epoxy bond, testing until failure. The EPDM 60A and PBD/NR 60A spines both suffered a bond failure during a 3.4-m/s impact. The PBD/NR 75A spine survived a 3.4-m/s hit and then had a bond failure at a 4.4-m/s hit. The EPDM 75A spine survived 3.4-, 4.4-,

5.5-, and 6.0-m/s hits. No testing was done beyond 6.0 m/s due to limitations of the instrumentation. All of the failures that were observed at these higher impact speeds were failures of the bond between the rubber and the epoxy adhesive.

Including the pretest materials demonstrator and the other 5 materials demonstrators, 35 of the 36 planned test hits were completed, along with an additional 9 hits at impact speeds above BRC levels, for a total of 44 test hits. After testing was completed, MCW generated a quick look report including preliminary data from the testing. Once all of the test data were compiled, MCW passed all data files to JHU/APL for analysis and use in validating the lumbar spine FEA model.

Once all of the test data were received, JHU/APL proceeded to analyze the data, making comparisons between the responses of the different Lumbar Spine Materials Demonstrators.

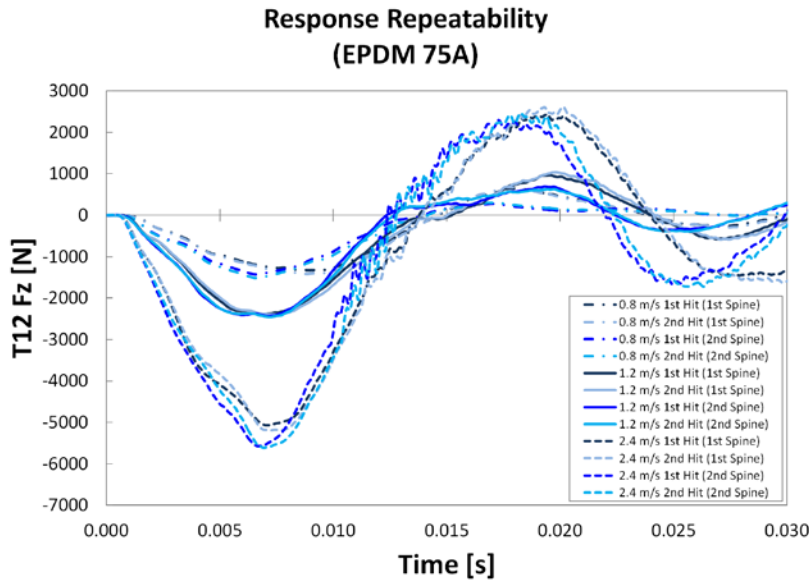
One aspect that was examined was intracomponent repeatability, that is, how much did the response vary from the first and second hits on each spine. The responses (vertical force at the upper load cell) for one of the EPDM 75A spines for all 6 of the planned hits are plotted in Fig. 21. The plot shows that the responses for each pair of hits are very similar to each other. The peak compressive loads between each pair of hits were found to be within 6% of each other.



Note: Data plotted is transformed and mass compensated, but not time shifted to match BRCs.

Fig. 21 Intracomponent repeatability

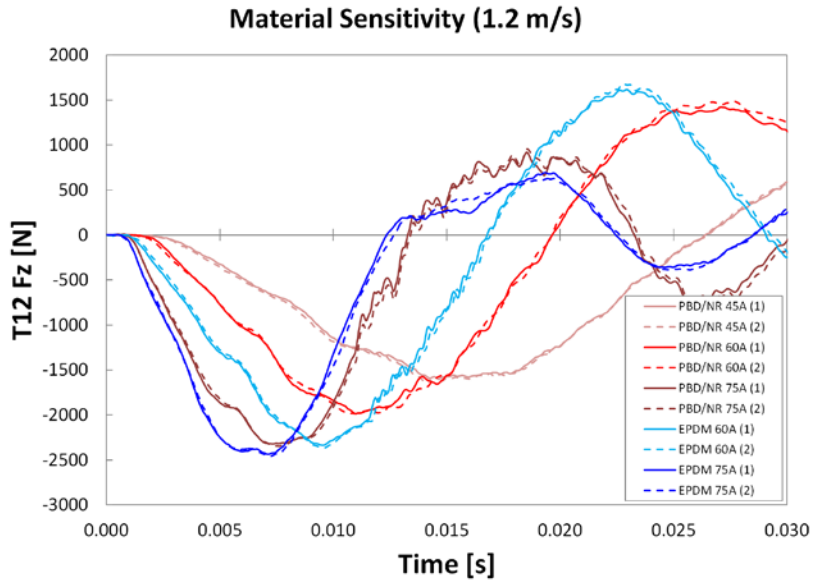
A similar plot is provided in Fig. 22 showing the intercomponent repeatability for the 2 EPDM 75A spines. Again, the peak loads (vertical force at the upper load cell) across both spines at the same speeds are similar, although a phase difference can be seen between the 2 spines as the response enters the tension phase.



Note: Data plotted is transformed and mass compensated, but not time shifted to match BRCs.

Fig. 22 Intercomponent repeatability

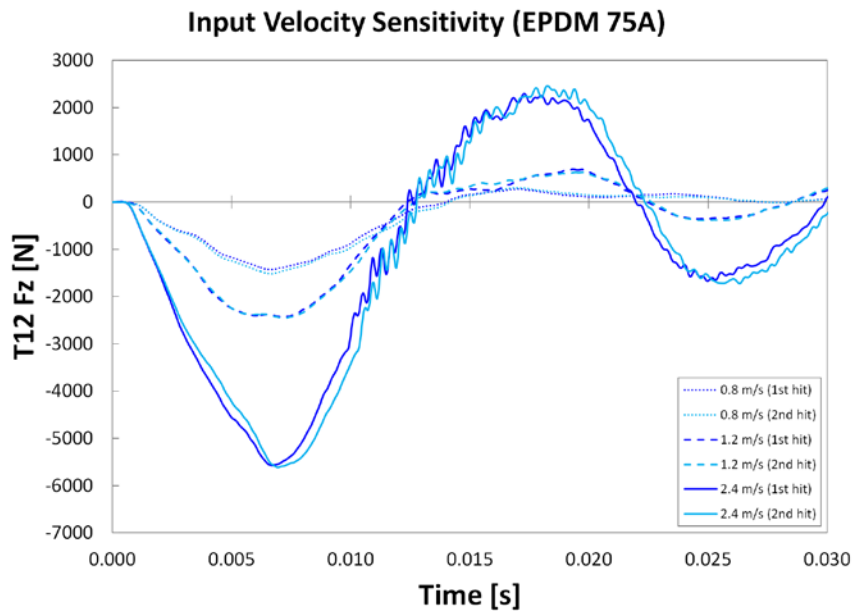
The sensitivity of the response to the compliant material used in the lumbar spine was also examined. Plots of the vertical force at the upper load cell for the 5 different compliant materials are shown in Fig. 23. This plot demonstrates that the material family and material hardness both have an effect on the dynamic response of the spine.



Note: Data plotted is transformed and mass compensated, but not time shifted to match BRCs.

Fig. 23 Response sensitivity to compliant material

As can be expected, the input velocity had a significant effect on the response of the spine. Figure 24 shows how the peak load increases with increasing impact speed.



Note: Data plotted is transformed and mass compensated, but not time shifted to match BRCs.

Fig. 24 Response sensitivity to impact speed

The data from the VertAc testing were also compared to the BRCs. To make these comparisons, the data first had to be processed to transfer the loads and moments to the same anatomical location that was used for the BRC data. This data processing consisted of 3 operations: mass compensation, moment transformation, and time shift.

The first step was to compensate the load data to take into account the difference in mass between the desired anatomical reference point and the load cell's location. Figure 25 illustrates the required mass compensation for both a PMHS-tested lumbar spine and a tested Lumbar Spine Materials Demonstrator. Equation 3 was used to transfer the load from the load cell to L1.

$$F' = F_z - M_{comp} * A_z, \quad (3)$$

in which F' is the mass compensated force in the global Z direction at the center of the T12/L1 joint, F_z is the measured force in in Z direction from the top load cell, M_{comp} is the compensation mass which consists of all the mass in between the center of the top load cell and the T12/L1 joint center, and A_z is the Z acceleration for the compensation mass.

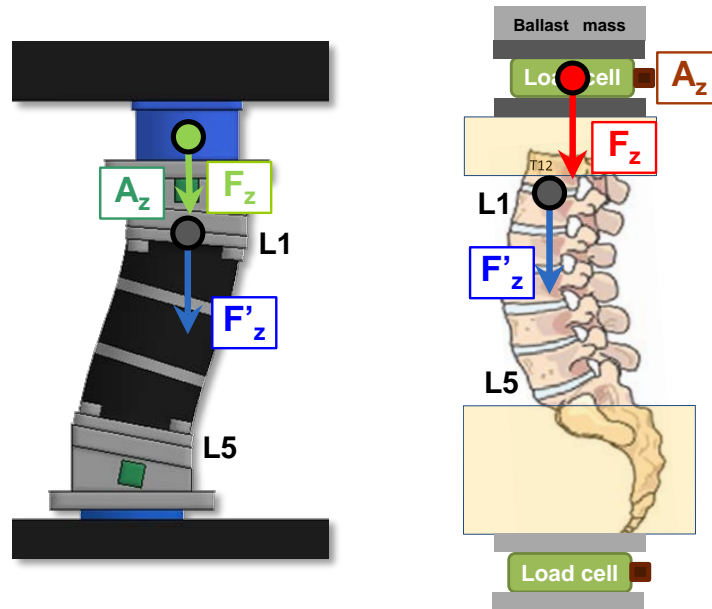


Fig. 25 Mass compensation of lumbar spine VertAc data

Similar to the force data, the moment data also had to be transferred to the desired location on the lumbar spine for both the PMHS testing and the materials demonstrator testing. Figure 26 illustrates this transformation for the moment data. Equation 4 was used for the moment transformation. The dimensions used for the moment transformations are shown and listed in Figs. 27 and 28.

$$M'_y = M_y + \vec{F} \times \vec{D} = M_y + F'_z D_x - F_x D_z, \quad (4)$$

in which M'_y is the transformed bending moment about the global Y axis at the T12/L1 joint center, M_y is the measured bending moment about the Y axis from the top load cell, F' is the mass compensated force in the global Z direction at the center of the T12/L1 joint, D_x is the transfer distance in the global X direction between the center of the top load cell and the T12/L1 joint center, F_x is the force in the X direction measured at the load cell, and D_z is the transfer distance in the global Z direction between the center of the top load cell and the T12/L1 joint center.

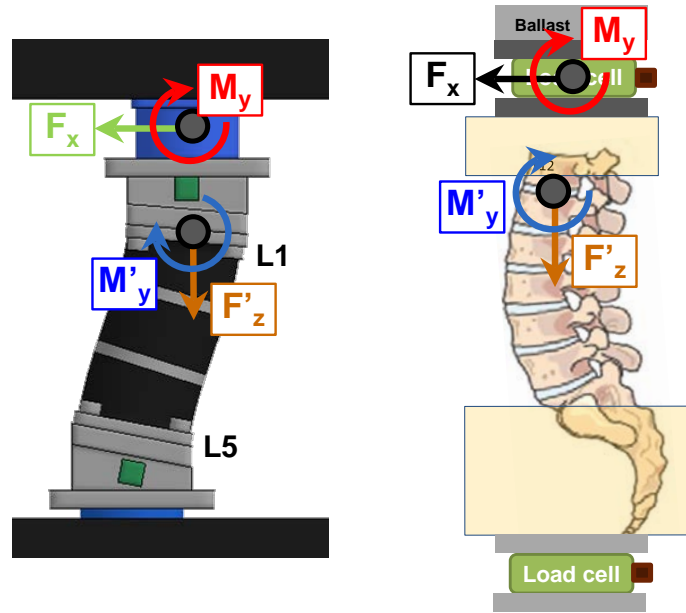


Fig. 26 Moment transformation of lumbar spine VertAc data

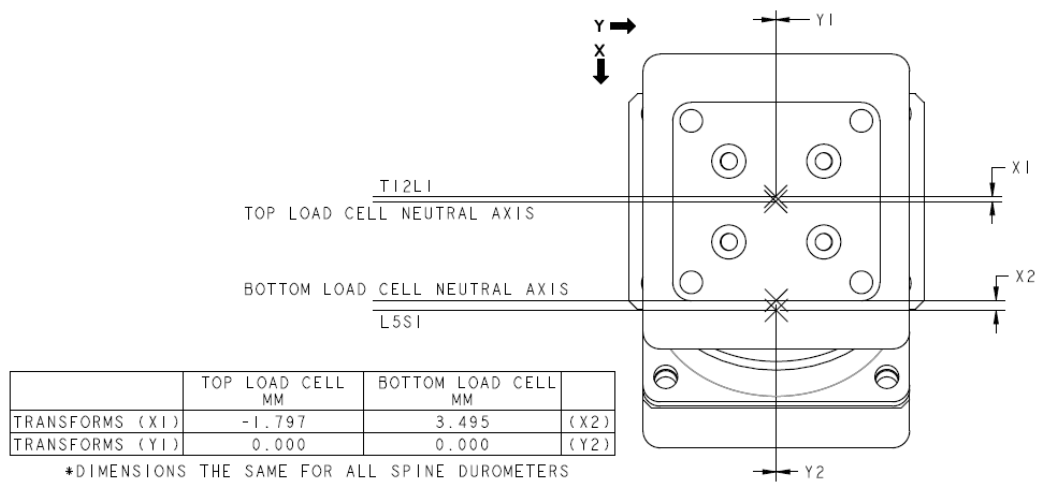


Fig. 27 Moment transformation dimensions in X and Y

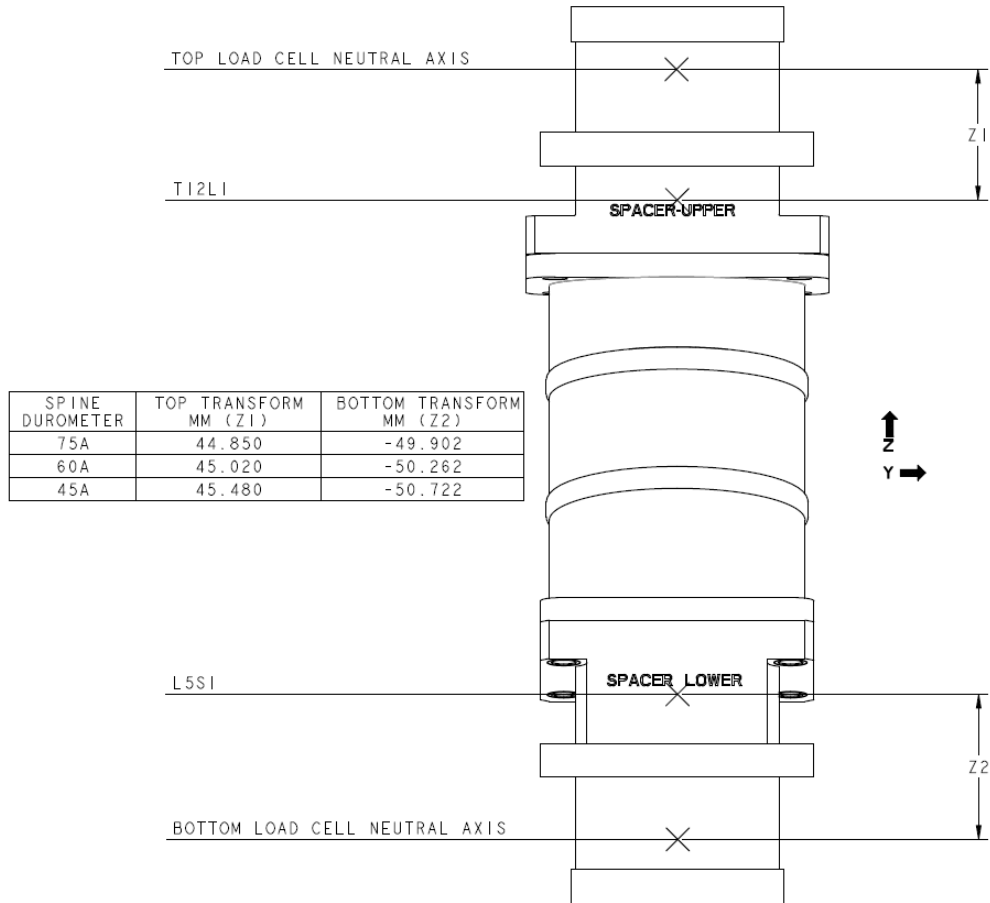


Fig. 28 Moment transformation dimensions in Z

The final step in the processing of the test data to make it comparable to the BRC data is to shift the time data. Because of inevitable differences in test setup (differences from time of data acquisition trigger to time of event), the materials demonstrator test data must be time shifted such that the even start points in the data correspond to the BRC event start times. The time shift for the materials demonstrator data was achieved by incrementally shifting the data forward and backward and then calculating the cross-correlation coefficient (CCC) with the average PMHS response until the maximum CCC was achieved.

Once the data were compensated, transformed, and time shifted, it was compared to the BRCs by plotting the responses (vertical force and moment) and generating CORA scores. Figures 29 and 30 show the processed data from the VertAc testing plotted against the BRC corridors for the 1.2-m/s impact speed. The data plotted are from the upper load cell and were transferred to the L1 location of the lumbar spine to be consistent with the BRC curves. These plots show that the vertical force

(Fz) plots correlate well, but the moment (My) plots are not showing the same magnitudes as the BRCs. Additional BRC comparison plots are provided in the Appendix.

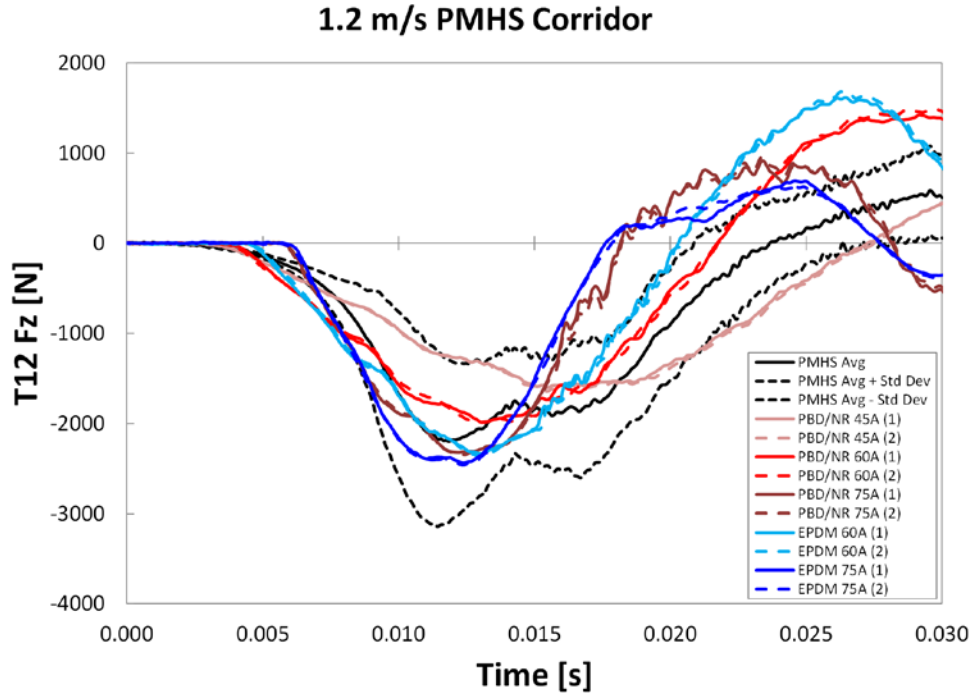


Fig. 29 Vertical force responses at L1/T12 compared to BRC for 1.2 m/s

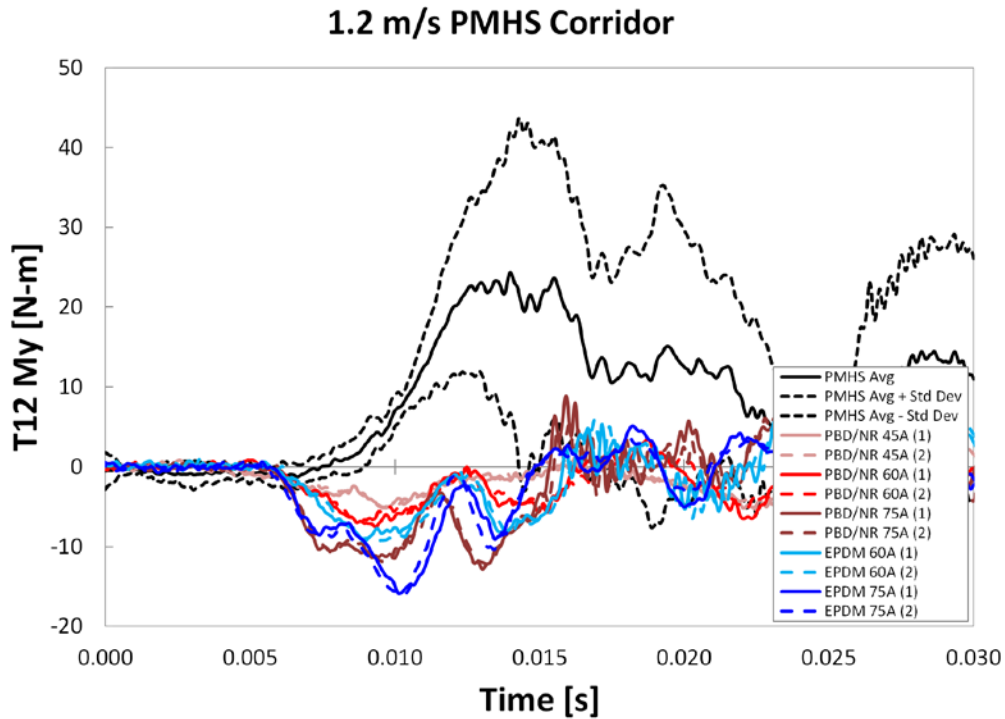


Fig. 30 Moment responses at L1/T12 compared to BRC for 1.2 m/s

The processed data for every test hit were compared to the BRCs and CORA scores were generated to rank how the different compliant materials stack up against the BRCs. The CORA scores for these comparisons are provided in Table 15. These CORA scores were generated in accordance with guidance from Pietsch et al.¹⁰ Table 16 provides the size CORA scores for comparing the size of the MCW testing data traces to the size of the BRC trace.

The highest average overall CORA score was found to be 0.64 and corresponded to the PBD/NR 45A Lumbar Spine Materials Demonstrator. This means that if one of the tested materials had to be chosen for use in the final ATD design, the PBD/NR 45A compliant material would provide the closest match to the BRCs out of those that were tested.

Looking at the size CORA scores, the highest-weighted average was found to be 0.60. This weighted average corresponded to both the PBD/NR 60A and EPDM 75A test data.

Table 15 MCW testing overall CORA scores for comparison to BRCs

Candidate materials	Test name	L5 force	L1/T12 force	L5 moment	L1/T12 moment
PBD/NR 45A weighted average = 0.64	V1 hit 1	0.75	0.66	0.65	0.37
	V1 hit 2	0.76	0.66	0.64	0.35
	V2 hit 1	0.79	0.82	0.65	0.51
	V2 hit 2	0.79	0.80	0.66	0.52
	V3 hit 1	0.67	0.61	0.52	0.53
PBD/NR 60A weighted average = 0.58	V1 hit 1	0.77	0.70	0.51	0.32
	V1 hit 2	0.79	0.69	0.50	0.31
	V2 hit 1	0.71	0.74	0.61	0.36
	V2 hit 2	0.71	0.73	0.65	0.35
	V3 hit 1	0.58	0.60	0.47	0.38
	V3 hit 2	0.50	0.55	0.47	0.54
PBD/NR 75A weighted average = 0.48	V1 hit 1	0.61	0.52	0.66	0.45
	V1 hit 2	0.63	0.55	0.65	0.43
	V2 hit 1	0.47	0.63	0.67	0.37
	V2 hit 2	0.48	0.64	0.67	0.36
	V3 hit 1	0.40	0.44	0.48	0.39
	V3 hit 2	0.34	0.37	0.48	0.39
EPDM 60A weighted average = 0.53	V1 hit 1	0.69	0.62	0.68	0.34
	V1 hit 2	0.70	0.59	0.67	0.32
	V2 hit 1	0.61	0.65	0.51	0.36
	V2 hit 2	0.62	0.65	0.48	0.36
	V3 hit t 1	0.55	0.56	0.48	0.39
	V3 hit 2	0.51	0.53	0.47	0.38
EPDM 75A weighted average = 0.53	V1 hit 1	0.64	0.59	0.57	0.34
	V1 hit 2	0.66	0.63	0.58	0.42
	V2 hit 1	0.52	0.65	0.66	0.40
	V2 hit 2	0.52	0.66	0.65	0.40
	V3 hit 1	0.39	0.44	0.60	0.42
	V3 hit 2	0.58	0.58	0.58	0.58

Note: Weights for scoring applied according to W0032. Highlighted materials provided the highest average CORA scores.

Table 16 MCW testing size CORA scores for comparison to BRCs

Candidate materials	Test name	L5 force	L1/T12 force	L5 moment	L1/T12 moment
PBD/NR 45A weighted average = 0.54	V1 hit 1	0.570	0.620	0.504	0.032
	V1 hit 2	0.597	0.646	0.484	0.038
	V2 hit 1	0.694	0.718	0.954	0.041
	V2 hit 2	0.698	0.744	0.973	0.039
	V3 hit 1	0.994	0.979	0.942	0.109
PBD/NR 60A Weighted Average = 0.60	V1 hit 1	0.921	0.806	0.517	0.082
	V1 hit 2	0.959	0.854	0.582	0.080
	V2 hit 1	0.791	0.924	0.607	0.098
	V2 hit 2	0.773	0.898	0.671	0.084
	V3 hit 1	0.601	0.766	0.817	0.091
	V3 hit 2	0.633	0.795	0.723	0.076
PBD/NR 75A weighted average = 0.59	V1 hit 1	0.965	0.743	0.806	0.378
	V1 hit 2	0.980	0.788	0.772	0.401
	V2 hit 1	0.810	0.950	0.664	0.280
	V2 hit 2	0.799	0.965	0.698	0.260
	V3 hit 1	0.488	0.633	0.410	0.223
	V3 hit 2	0.485	0.636	0.389	0.244
EPDM 60A weighted average = 0.57	V1 hit 1	0.981	0.982	0.992	0.149
	V1 hit 2	0.986	0.954	0.957	0.146
	V2 hit 1	0.727	0.753	0.413	0.135
	V2 hit 2	0.716	0.738	0.365	0.153
	V3 hit 1	0.555	0.591	0.488	0.114
	V3 hit 2	0.569	0.608	0.470	0.122
EPDM 75A weighted average = 0.60	V1 hit 1	0.700	0.593	0.323	0.245
	V1 hit 2	0.754	0.676	0.334	0.263
	V2 hit 1	0.979	0.908	0.783	0.229
	V2 hit 2	0.958	0.926	0.759	0.234
	V3 hit 1	0.567	0.650	0.946	0.168
	V3 hit 2	0.591	0.591	0.591	0.591

Note: Weights for scoring applied according to W0032. Highlighted materials provided the highest average CORA scores.

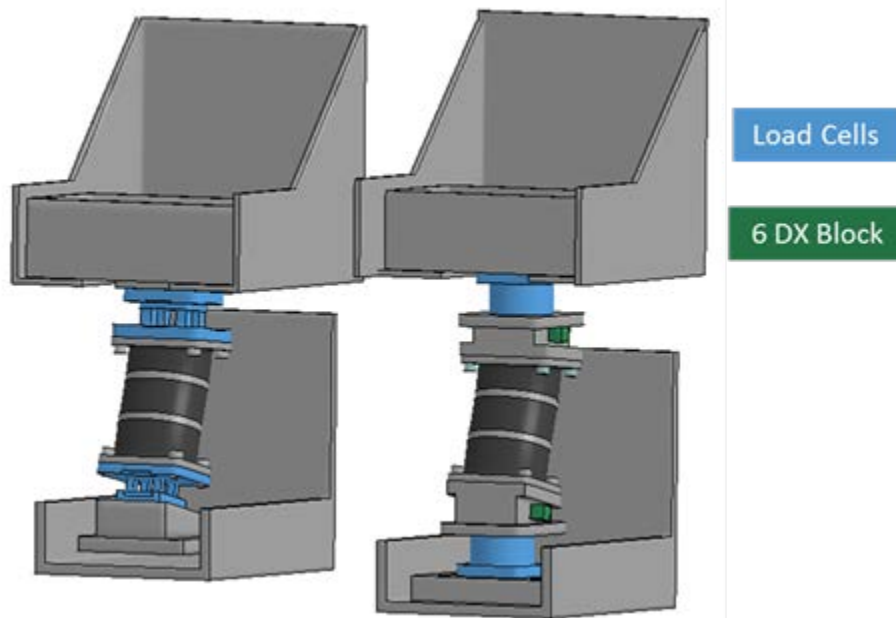
6. Modeling and Simulation Validation

6.1 Model Refinement

FEM interface components used to attach the WIAMan lumbar spine to the VertAc test rig were modified leveraging CAD from fabricated parts. Three sets of interface pieces were meshed to match the 3 separate interfaces used experimentally to

Approved for public release; distribution is unlimited.

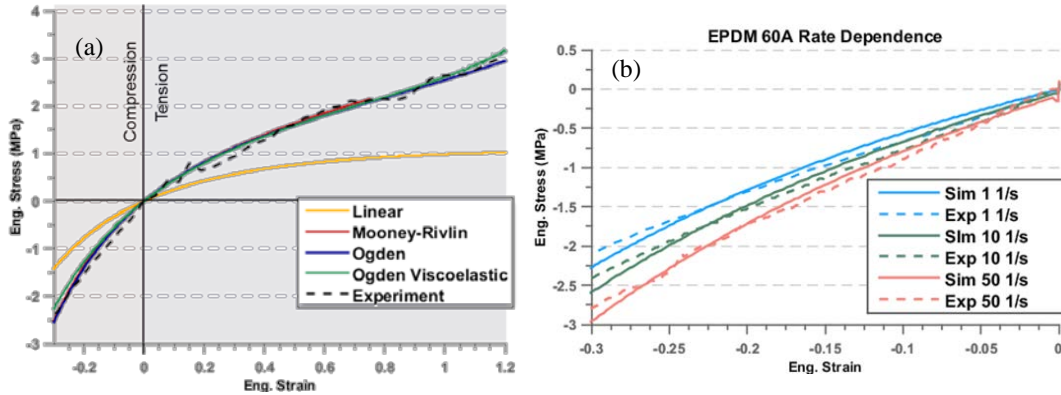
ensure consistent masses between impacts of lumbar prototypes with varying densities (Fig. 31). Masses were calculated from the updated model and compared against newly fabricated parts, including the interface pieces and WIAMan lumbar prototype, which were unavailable during earlier simulations. The total mass differed by less than 0.5%. Virtual accelerometers were employed in the model to compare to experimental traces, with acceleration output from the nodes defining the accelerometer block, using LS-DYNA's constrained interpolation method.



Note: (Left) nominal configuration. (Right) VertAc rig configuration.

Fig. 31 WIAMan lumbar spine FEM

Constitutive models of varying complexity were fit to materials characterization data for each of the 5 fabricated lumbar spine materials (PBD/NR 45A, PBD/NR 60A, PBD/NR 75A, EPDM 60A, and EPDM 75A). Stress-strain curves at multiple rates were generated from uniaxial tension and compression of single fully integrated LS-DYNA hexahedral elements. A simple linear-elastic material model was included as a control case, while hyperelastic constitutive models including Mooney-Rivlin and Ogden resulted in close agreement to experimental characterization (Fig. 32). Only the Ogden viscoelastic material model reproduced the rate-dependence and hysteretic response observed from Instron testing (Fig. 32).



Note: a) Plotted for several material models. b) Plotted for the Ogden viscoelastic material model at multiple rates.

Fig. 32 Single element stress-strain results for EPDM 60 Shore A

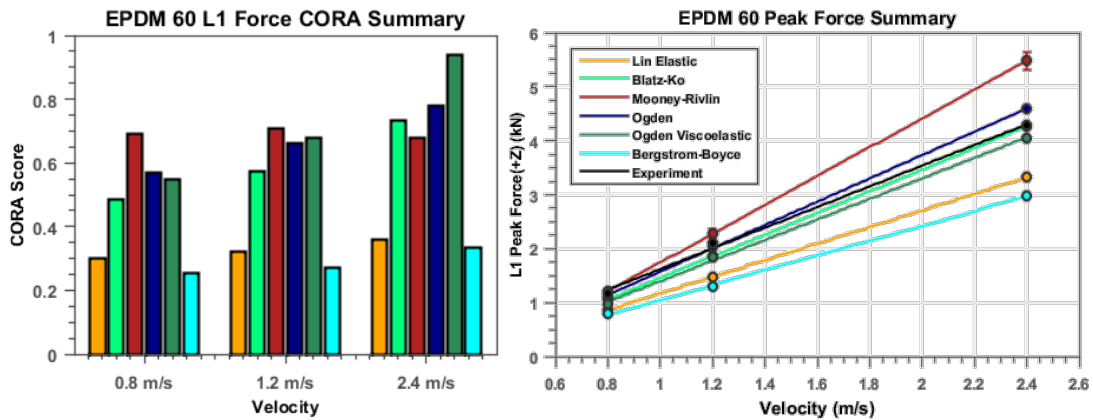
6.2 Model Correlation to VertAc Test Results

The WIAMan lumbar spine FEM was vertically loaded in the VertAc rig according to Table 17. Six separate material models were used to simulate the full range of EPDM 60A experiments, while 3 were used to simulate EPDM 75A, PBD/NR 45A, PBD/NR 60A, and PBD/NR 75A. Failure cases were excluded from the simulation matrix.

Table 17 Simulation matrix for material exploration

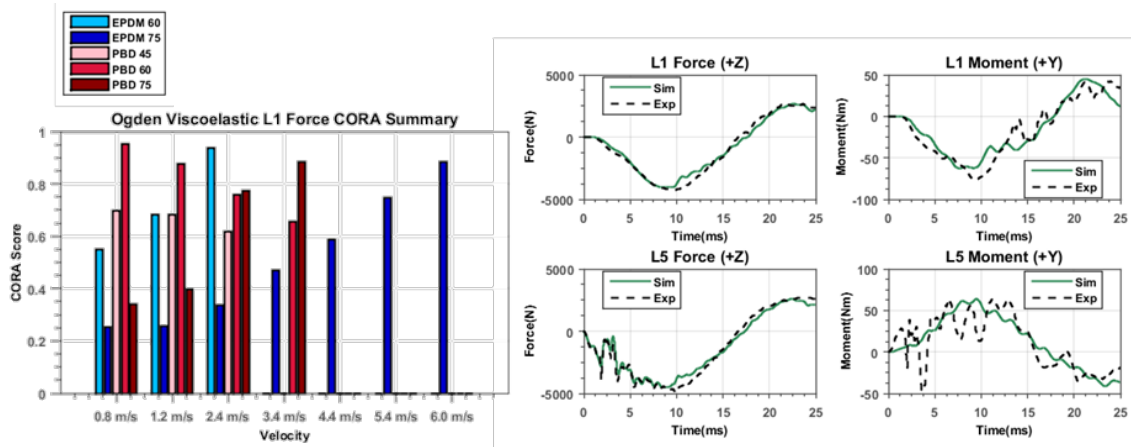
Material	DYNA material model	Carriage velocity data sets
EPDM 75A	Mooney-Rivlin	V1 (4x), V2 (4x), V3 (4x), V4 (2x), V5 (1x), V6 (1x), V7 (1x)
	Ogden	V1 (4x), V2 (4x), V3 (4x), V4 (2x), V5 (1x), V6 (1x), V7 (1x)
	Ogden Viscoelastic	V1 (4x), V2 (4x), V3 (4x), V4 (2x), V5 (1x), V6 (1x), V7 (1x)
EPDM 60A	Linear Elastic	V1 (2x), V2 (2x), V3 (2x), V4 (1x)
	Blatz-Ko	V1 (2x), V2 (2x), V3 (2x), V4 (1x)
	Mooney-Rivlin	V1 (2x), V2 (2x), V3 (2x), V4 (1x)
	Ogden	V1 (2x), V2 (2x), V3 (2x), V4 (1x)
	Ogden Viscoelastic	V1 (2x), V2 (2x), V3 (2x), V4 (1x)
	Bergstrom-Boyce	V1 (2x), V2 (2x), V3 (2x), V4 (1x)
PBD/NR 75A	Mooney-Rivlin	V1 (2x), V2 (2x), V3 (2x), V4 (1x), V5 (1x)
	Ogden	V1 (2x), V2 (2x), V3 (2x), V4 (1x), V5 (1x)
	Ogden Viscoelastic	V1 (2x), V2 (2x), V3 (2x), V4 (1x), V5 (1x)
PBD/NR 60A	Mooney-Rivlin	V1 (2x), V2 (2x), V3 (2x), V4 (1x)
	Ogden	V1 (2x), V2 (2x), V3 (2x), V4 (1x)
	Ogden Viscoelastic	V1 (2x), V2 (2x), V3 (2x), V4 (1x)
PBD/NR 45A	Mooney-Rivlin	V1 (2x), V2 (2x), V3 (1x)
	Ogden	V1 (2x), V2 (2x), V3 (1x)
	Ogden Viscoelastic	V1 (2x), V2 (2x), V3 (1x)

Results from the EPDM 60 (Fig. 33) simulation indicate that the Ogden viscoelastic material model is the ideal model for accurate predictions. While the Blatz-Ko model matched peak forces better than any other material model (Fig. 33, right), the lack of material damping meant that unloading was not predicted well. The Ogden viscoelastic material model produced the highest CORA scores on average, including a CORA score above 0.9 for the 2.4-m/s case (Fig. 33, left). Furthermore, unloading was predicted using the Ogden viscoelastic model, as can be seen from the characteristic results in Fig. 34. Moment results were predicted well using the Ogden viscoelastic material model (Fig. 34, right). The high-frequency content observed in the L5 moment plot was not reproduced, likely because carriage oscillations were constrained in the simulation via the velocity boundary condition.



Note: (Left) CORA score calculated for each material type at each BRC velocity, (Right) peak transmitted force compared to simulation average for each material type.

Fig. 33 EPDM 60 simulation results summary



Note: (Left) Summary of CORA scores comparing L1 force from simulations using Ogden viscoelastic material model against corresponding experiments, across range of velocities and material types. (Right) EPDM 60, 2.4 m/s experimental results compared against simulations using Ogden viscoelastic material models.

Fig. 34 Ogden viscoelastic simulation results summary

Figure 34, left, summarizes the accuracy of the Ogden viscoelastic material model in predicting experimental results. CORA scores were generated using the default parameters, where a higher score indicates a closer correspondence to the experiment. In general, predictive capability increases with velocity, and decreases with Shore A durometer. All simulation except for the EPDM 75 and PBD/NR 75 simulations at 0.8, 1.2, and 2.4 m/s produced CORA scores above 0.5.

6.3 Model Predictive Results

Following the material exploration detailed in Section 6.2, the efficacy of the Ogden viscoelastic material model was tested via a blind comparison to experimental results for a variety of conditions (Table 18). Experimental velocity traces from the lower carriage were provided as model inputs, while all other channels were withheld for a blind comparison.

After running the simulations, experimental results were released and compared to the blind predictions using CORA (Tables 19 and 20). Again, CORA decreased with material stiffness. Overall, CORA scores were relatively high, reaching above 0.5 for 20 of the 24 cases, and above 7.5 for 11 of the 24 cases.

The validated WIAMan lumbar FEM will increase confidence in simulations where accompanying experimental data are not available, including assessing lumbar response at higher velocities, response variation due to geometrical changes, and material optimization studies.

Table 18 Blind validation experiments

Test name	Material	Velocity (m/s)
EPDM60_v2p5_1	EPDM 60 Shore A	1.8
EPDM60_v2p5_2	EPDM 60 Shore A	1.8
EPDM75_v2p5_1	EPDM 75 Shore A	1.8
EPDM75_v2p5_2	EPDM 75 Shore A	1.8
EPDM75X_v3p5_1	EPDM 75 Shore A	1.8
EPDM75X_v3p5_2	EPDM 75 Shore A	1.8
PBD45_v2p5_1	PBD 45 Shore A	1.8
PBD45_v2p5_2	PBD 45 Shore A	1.8
PBD60_v2p5_1	PBD 60 Shore A	1.8
PBD60_v2p5_2	PBD 65 Shore A	1.8
PBD75_v2p5_1	PBD 75 Shore A	1.8
PBD75_v2p5_2	PBD 75 Shore A	1.8

Table 19 L1 force CORA score breakdown for blind validation cases

Test name	L1 force (+Z) CORA overall	L1 force (+Z) CORA size	L1 force (+Z) CORA progression	L1 force (+Z) CORA cross correlation
EPDM60_v2p5_1	0.850	0.770	0.930	0.850
EPDM60_v2p5_2	0.867	0.789	0.945	0.867
EPDM75_v2p5_1	0.505	0.862	0.148	0.505
EPDM75_v2p5_2	0.532	0.954	0.110	0.532
EPDM75X_v3p5_1	0.717	0.928	0.506	0.717
EPDM75X_v3p5_2	0.716	0.929	0.503	0.716
PBD45_v2p5_1	0.757	0.839	0.675	0.757
PBD45_v2p5_2	0.756	0.831	0.682	0.756
PBD60_v2p5_1	0.877	0.848	0.906	0.877
PBD60_v2p5_2	0.862	0.837	0.888	0.862
PBD75_v2p5_1	0.728	0.961	0.496	0.728
PBD75_v2p5_2	0.762	0.927	0.597	0.762

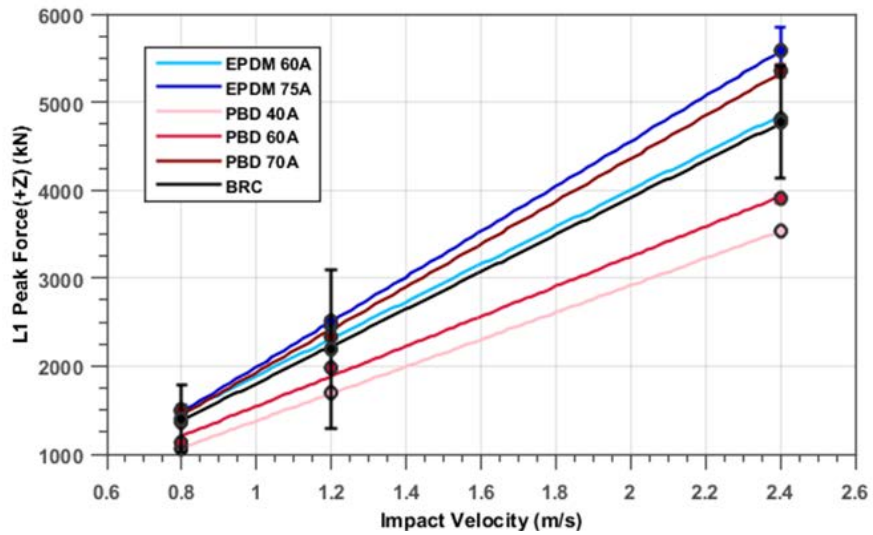
Table 20 L1 Moment CORA score breakdown for blind validation cases

Test name	L1 moment (+Y) CORA overall	L1 moment (+Y) CORA size	L1 moment (+Y) CORA progression	L1 moment (+Y) CORA cross correlation
EPDM60_v2p5_1	0.687	0.692	0.682	0.687
EPDM60_v2p5_2	0.674	0.699	0.650	0.674
EPDM75_v2p5_1	0.473	0.804	0.143	0.473
EPDM75_v2p5_2	0.449	0.764	0.134	0.449
EPDM75X_v3p5_1	0.466	0.624	0.309	0.466
EPDM75X_v3p5_2	0.466	0.635	0.296	0.466
PBD45_v2p5_1	0.790	0.993	0.588	0.790
PBD45_v2p5_2	0.786	0.994	0.578	0.786
PBD60_v2p5_1	0.863	0.925	0.802	0.863
PBD60_v2p5_2	0.845	0.908	0.782	0.845
PBD75_v2p5_1	0.612	0.851	0.373	0.612
PBD75_v2p5_2	0.597	0.820	0.374	0.597

6.4 Model Correlation to BRCs

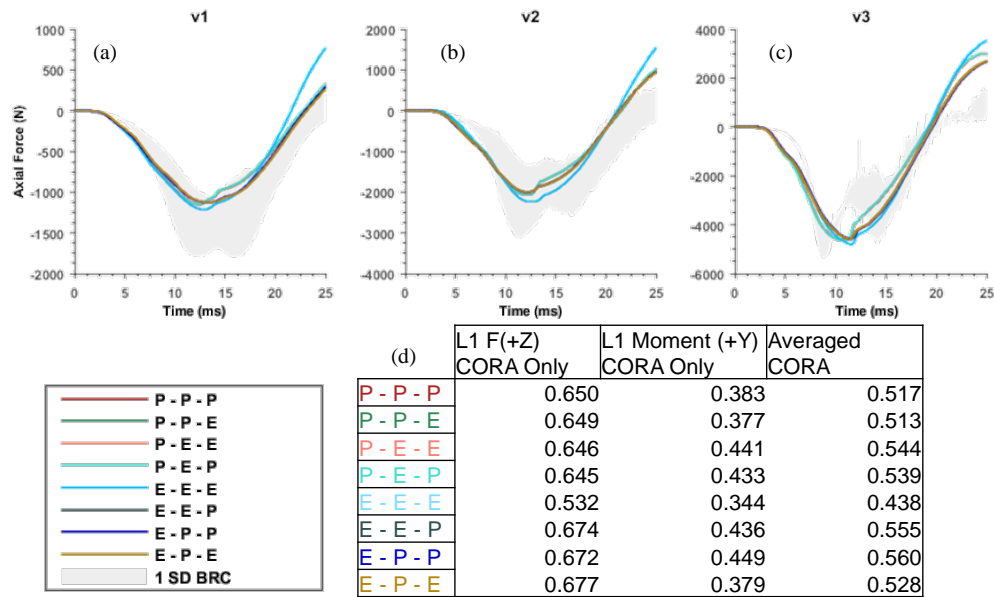
An initial optimization study was conducted to explore the effect of varying the lumbar spine material properties at each of the three puck levels. To limit the number of material types that could be used, experimental ATD peak force was plotted against BRC peak force for each material type (Fig. 35). For each velocity, EPDM 60 was the nearest bound above the BRC values, while PBD/NR 60 was the nearest lower bound. With this in mind, puck type was varied between EPDM 60 and PBD/NR 60 at each puck level, resulting in 8 possible permutations. Each of these permutations was run at all 3 BRC velocities, for a total of 24 simulations. Figure 36 summarizes the results.

Top performers from this discrete optimization study were picked as either the highest L1 axial force CORA score, the highest L1 bending moment CORA score, or an average of the 2 scores. Looking at L1 force, E – P – E was the best combination, resulting in a CORA score of 0.677, up from 0.532 from an E – E – E lumbar spine. For L1 bending moment, E – P – P had a high CORA score of 0.449, compared to 0.383 for P – P – P. Finally, E – P – P resulted in the largest average CORA score of 0.560, up from 0.517 for P – P – P. Overall, CORA scores were most sensitive to changes in the puck material of the lowest puck position.



Note: Peak force compared to BRC peak force across variety of material types and boundary conditions. Error bars represent standard deviation between repeat tests.

Fig. 35 ATD peak force compared to BRC peak force



Note: Legend code lists puck type from bottom to top, E is EPDM 60 and P is PBD/NR 60. (Top) L1 axial force traces compared against BRCs at a) 0.8 m/s, b) 1.2 m/s, and c) 2.4 m/s. d) Table of CORA scores, averaged across each velocity.

Fig. 36 Results of varying material type at each spinal level

7. Conclusions and Recommendations

The Lumbar Spine Materials Demonstrator effort had 3 primary objectives. The first was to generate experimental data that could be used to validate the FEM of the lumbar spine so that it can be used as a tool to inform the design of the WIAMan ATD. The second objective was to create Lumbar Spine Materials Demonstrators using the FEM to select compliant materials. These materials demonstrators could then be used to characterize candidate materials, evaluate the sensitivity of the ATD lumbar spine response to material parameters, and collect the data required to accomplish the first objective. The final objective was to compare the Lumbar Spine Materials Demonstrator responses to the BRCs and see how close the design and selected materials match the PMHS testing responses.

The FEM of the lumbar spine was used in conjunction with the previously validated VertAc rig FEM to perform a preliminary optimization of the compliant material for the lumbar spine. By simulating the BRC test conditions and comparing the simulated responses to the preliminary BRCs, an optimized material hardness was selected. Given that no simulation is perfect, a range of hardnesses were chosen from 2 different rubber families to be built and tested.

With the materials selected, the next step was to fabricate the materials demonstrators and test them on the VertAc. The VertAc test data, combined with the individual material characterization data, were used to validate the FEM,

ensuring that the simulation output accurately replicated the responses observed during the VertAc testing. During this validation process, several material models of varying complexity were used in the FEM. Using these various material models allowed the correct level of complexity to be selected to best match the responses from the testing. Of the material models used in the validation simulations, the Ogden viscoelastic model had the best correlation to the test data. Additional validation of the model can be pursued with other modeling options, but the model is considered validated and ready for use as needed for predictive studies.

Comparisons of the simulation peak force output and VertAc test data indicate that a hardness of around 60A will provide the closest match to the BRCs for the conditions tested. This aligns with the preliminary optimization, which pointed towards a hardness of approximately 65A. During comparison of the VertAc data to the BRCs, it was observed that the axial loading and flexion-extension moment response of the PBD/NR 45A lumbar spine best replicated PMHS response, in terms of overall CORA score (Table 16). While this differs from the conclusion of the FEM simulations, it should be noted that CORA size scores were closest for the 60A materials, agreeing with FEM peak force predictions. ATD to PMHS CORA scores resulted in relatively low moment scores, with peak moments from ATD testing lower, and often opposite in sign, compared to PMHS. The importance of the moment will be better known when the PMHS alternate posture tests are completed, but it is likely that the geometry and alignment of the test article in questions can lead to high variance in the moment response. In fact, one of the PMHS specimens produced an opposite sign T12-L1 moment response compared to the rest of the test series, bolstering this hypothesis. With this outcome, the FEM should be considered for evaluating lumbar spine design modifications to determine the effect of various parameters, including material and geometric changes, on the responses (both force and moment).

As follow-on to this effort, it is recommended that the validated FEM be used to optimize the material and geometry of the WIAMan lumbar spine to specifically match the BRCs. This new design could then be fabricated using the molded in place approach, and then it should be tested on the VertAc. The test data can then be compared to the test data from the BRCs to confirm that it indeed has a similar response.

8. References

1. WIAMan ATD Product Team. WIAMan project ATD technical data package. Manikin, 2014 Dec 3.
2. ASTM D575 - 91. Standard test methods for rubber properties in compression. West Conshohocken (PA): ASTM International; 2012.
3. ASTM D412 - 98a. Standard test methods for vulcanized rubber and thermoplastic elastomers—tension. West Conshohocken (PA): ASTM International; 1998.
4. Internal Quality Standard Operating Procedures JHU/APL Standard Q53-576. Surface preparation of aluminum alloys prior to adhesive bonding. Laurel (MD): Johns Hopkins University Applied Physics Laboratory; 2008.
5. Internal Quality Standard Operating Procedures JHU/APL Standard QF3-502. Application of BR-127 primer. Laurel (MD): Johns Hopkins University Applied Physics Laboratory; 2012.
6. Internal Quality Standard Operating Procedures JHU/APL Standard Q53-667. Fabrication and acceptance of adhesive bonded assemblies. Laurel (MD): Johns Hopkins University Applied Physics Laboratory; 2009.
7. ASTM D5592 - 96. Standard guide for dynamic testing of vulcanized rubber and rubber-like materials using vibratory methods. West Conshohocken (PA): ASTM International; 2011.
8. Internal Quality Standard Operating Procedures JHU/APL Standard Q53-599. Surface preparation of low carbon steel alloys prior to adhesive bonding. Laurel (MD): Johns Hopkins University Applied Physics Laboratory; 2008.
9. Gibson MW. WIAMan lumbar spine materials demonstrator test plan. v2.2. The Johns Hopkins University Applied Physics Laboratory, 2015 May 20.
10. Pietsch H, Smith T, Wiley K. W0032 biofidelity assessment scheme. V1.2. 2015 Nov 6.

Appendix. Additional Testing Data

A.1 Results Table for Lap-Shear Testing

Table A-1 Lap-shear testing results

Test no.	Rubber	Adhesive ^a	Coupon no.	Peak load (lbf)	Peak shear stress (psi)	Speed ^b (inches/min)	Rubber thickness (inches)	Failure mode
3	EPDM	Chemlok	1	529	217.5	0.118	0.1969	Cohesive - rubber
8	EPDM	Chemlok	2	650.9	267.7	0.118	0.1969	Cohesive - rubber
9	EPDM	Chemlok	3	245.8	101.1	0.118	0.1969	Cohesive - rubber
1	PBD	Chemlok	1	3647.4	1499.9	0.118	0.1969	Cohesive - rubber
6	PBD	Chemlok	2	3790.6	1558.8	0.118	0.1969	Cohesive - rubber
7	PBD	Chemlok	3	3558.3	1463.3	0.118	0.1969	Cohesive - rubber
4	EPDM	Hysol epoxy + BR 127	1	874.2	359.5	0.047	0.0787	Adhesive - rubber/epoxy
10	EPDM	Hysol epoxy + BR 127	2	989	406.7	0.047	0.0787	Adhesive - rubber/epoxy
11	EPDM	Hysol epoxy + BR 127	3	1009.7	415.2	0.047	0.0787	Adhesive - rubber/epoxy
2	PBD	Hysol epoxy + BR 127	1	649.8	267.2	0.047	0.0787	Adhesive - rubber/epoxy
5	PBD	Hysol epoxy + BR 127	2	1163.8	478.6	0.047	0.0787	Adhesive - rubber/epoxy
12	PBD	Hysol epoxy + BR 127	3	780.5	321.0	0.047	0.0787	Adhesive - rubber/epoxy
13	EPDM	Hysol epoxy + CLP	1	2194.8	902.6	0.047	0.0790	Cohesive - rubber
14	EPDM	Hysol epoxy + CLP	2	1886.4	775.7	0.047	0.0790	Cohesive - rubber
15	EPDM	Hysol epoxy + CLP	3	2223.2	914.2	0.047	0.0790	Cohesive - rubber
16	PBD	Hysol epoxy + CLP	1	3987.5	1639.7	0.047	0.0790	Cohesive - rubber
17	PBD	Hysol epoxy + CLP	2	4027.8	1656.3	0.047	0.0790	Cohesive - rubber
18	PBD	Hysol epoxy + CLP	3	4086	1680.3	0.047	0.0790	Cohesive - rubber

^a“Chemlok” = Chemlok 205 primer with 220 adhesive, “Hysol Epoxy” = Hysol 9309.3NA epoxy, “BR 127” = BR 127 primer, “CLP” = Chemlok 7701 primer, PBD = Polybutadiene, EPDM = Ethylene propylene diene monomer

^bEngineering shear strain rate for all tests is 0.01 s⁻¹

A.2 Lumbar Spine Materials Demonstrator Comparison to Biofidelic Response Corridors (BRCs)

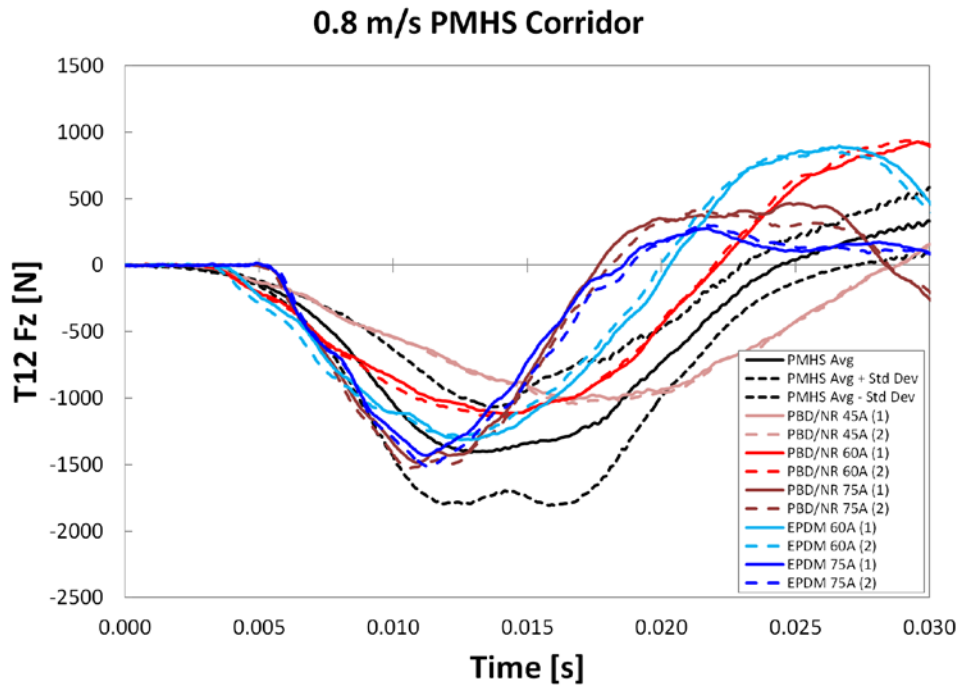


Fig. A-1 Vertical force BRC comparison for 0.8 m/s

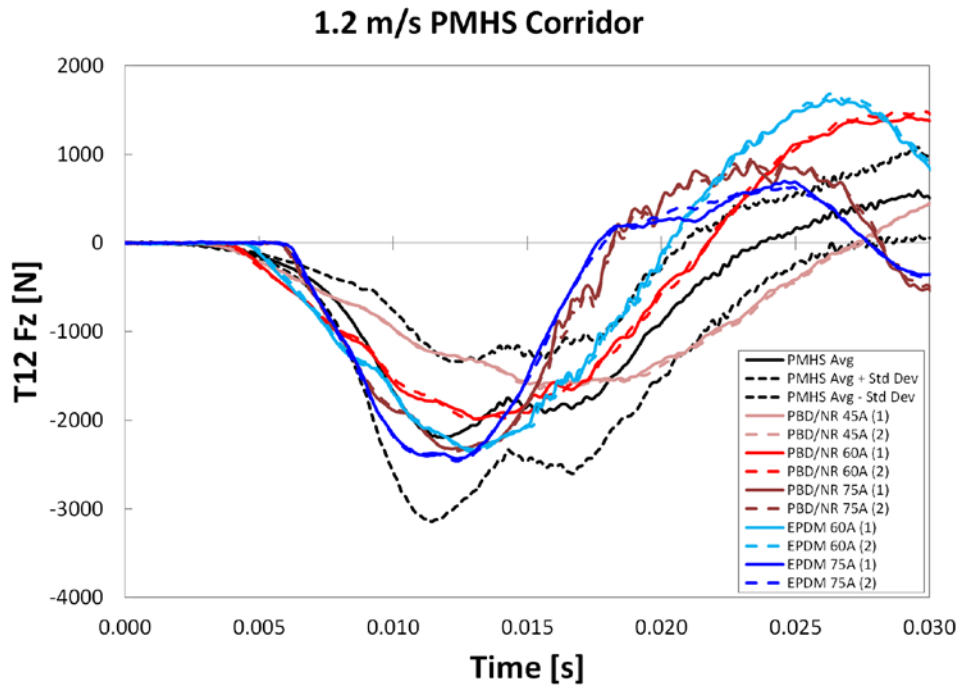


Fig. A-2 Vertical force BRC comparison for 1.2 m/s

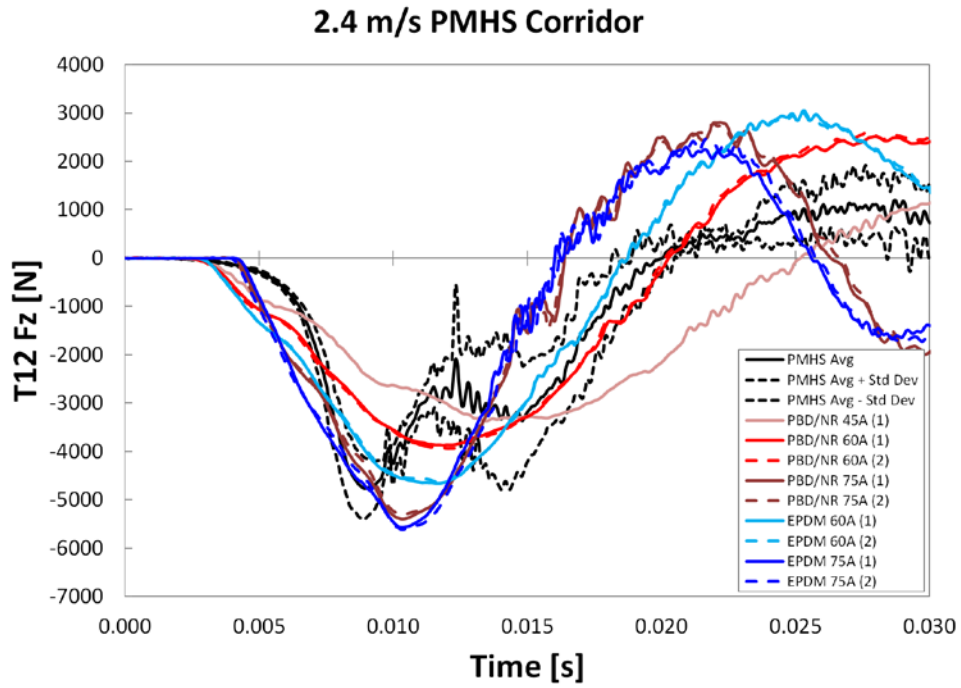


Fig. A-3 Vertical force BRC comparison for 2.4 m/s

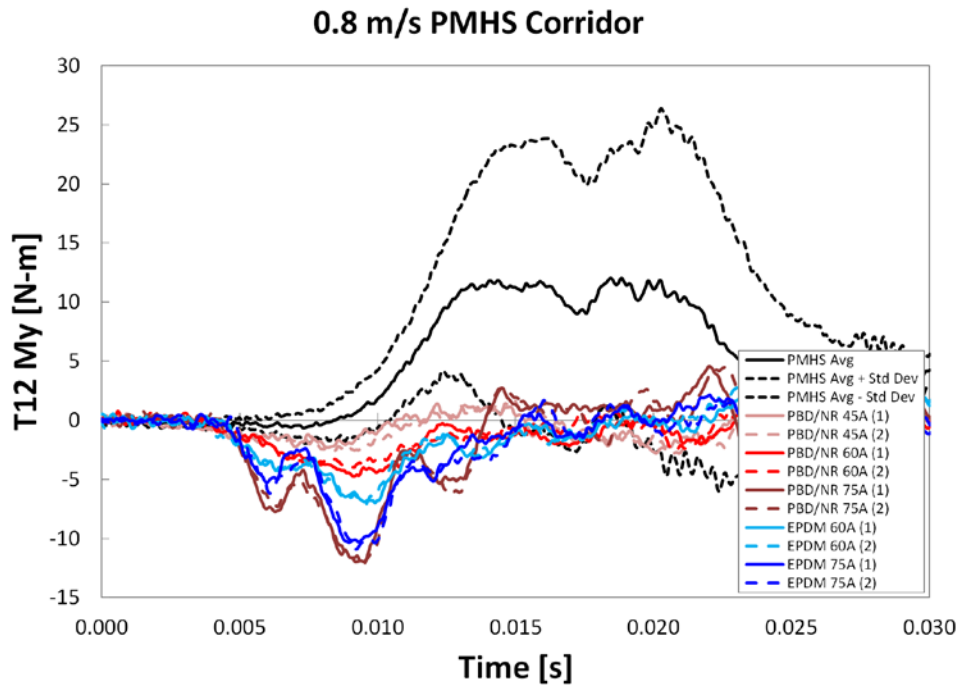


Fig. A-4 Moment BRC comparison for 0.8 m/s

1.2 m/s PMHS Corridor

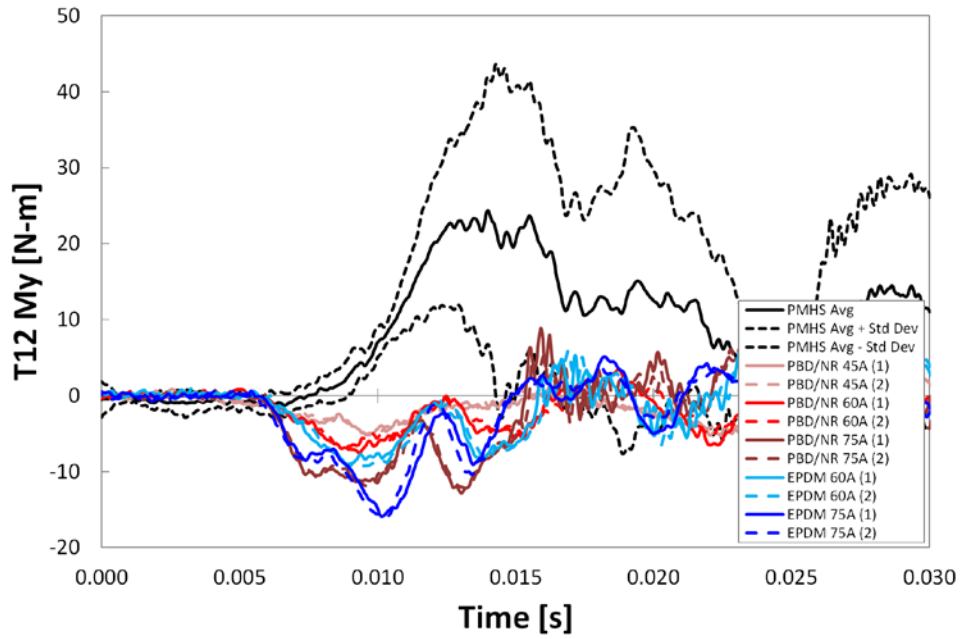


Fig. A-5 Moment BRC comparison for 1.2 m/s

2.4 m/s PMHS Corridor

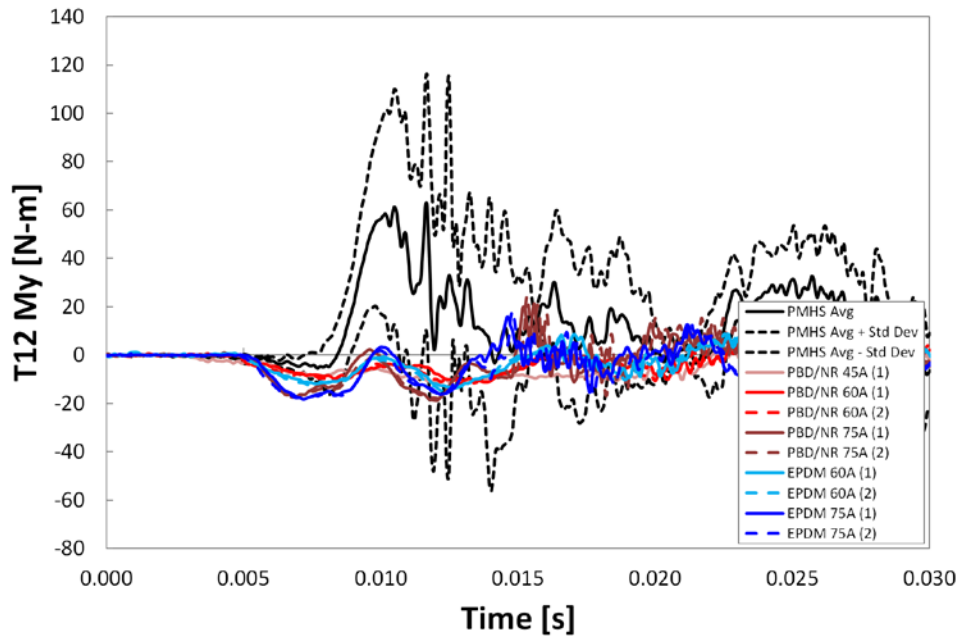


Fig. A-6 Moment BRC comparison for 2.4 m/s

INTENTIONALLY LEFT BLANK.

List of Symbols, Abbreviations, and Acronyms

3-D	3-dimensional
ARDL	Akron Rubber Development Laboratory
ATD	Anthropomorphic Test Device
BR	brominated butyl rubber
Br IIR	butyl rubber
BRC	Biofidelic Response Corridor
Buna-N	nitrile butadiene rubber
CAD	computer-aided design
CCC	cross-correlation coefficient
CORA	Correlation and Analysis
DMA	dynamic mechanical analysis
DOD	Department of Defense
EPDM	ethylene propylene fiene monomer
EUT	equipment under test
FEA	finite element analysis
FEM	finite element model
FDM	fused deposition modeling
fps	frames per second
GPa	Gigapascal
IPA	isopropyl alcohol
JHU/APL	The Johns Hopkins University Applied Physics Laboratory
kg	kilogram
kHz	kilohertz
kN	kilonewton
lbf	pound force

m/s	meters per second
MCW	The Medical College of Wisconsin
MPa	megapascal
ms	millisecond
N	Newton
N-m	Newton-Meter
NBR	nitrile butadiene rubber
Pa	Pascal
PBD/NR	polybutadiene/natural rubber blend
PMHS	postmortem human subject
psi	pounds per square inch
PUR	polyurethane
s	second
SBR	styrene butadiene rubber
T _g	glass transition temperature
TDP	technical data package
UBB	under-body blast
VertAc	vertical accelerator
WIAMan	Warrior Injury Assessment Manikin

1 DEFENSE TECHNICAL
(PDF) INFORMATION CTR
DTIC OCA

2 DIRECTOR
(PDF) US ARMY RESEARCH LAB
RDRL CIO L
IMAL HRA MAIL & RECORDS
MGMT

1 GOVT PRINTG OFC
(PDF) A MALHOTRA

12 DIR USARL
(PDF) RDRL DPW
J TICE
RDRL SLB E
C BARKER
D HOWLE
M MAHAFFEY
RDRL WMM G
D CRAWFORD
J LENHART
RDRL WMP B
C HOPPEL
RDRL WMP F
M CHOWDHURY
N GNIAZDOWSKI
E FIORAVANTE
D KRAYTERMAN
RDRL WMP G
S KUKUCK

INTENTIONALLY LEFT BLANK.